MDPI (/)

Journals (/about/journals) Topics (/topics) Information (/authors) Author Services (/authors/services) Initiatives (/about/initiatives) About (/about)

(/toggle_desktop_layout_cookie)

Sign In / Sign Up (/user/login)

Submit (https://susy.mdpi.com/user/manuscripts/upload?journal=catalysts)

Search for Articles:

Title / Keyword

Author / Affiliation / Email

Catalysts

All Article Types

Search

Advanced Search

Journals (/about/journals) / Catalysts (/journal/catalysts) / Volume 16 (/2073-4344/16) / Issue 5 (/2073-4344/16/5) / 10.3390/catal16050468 /

catalysts

(/journal/catalysts)

Submit to this Journal (https://susy.mdpi.com/user/manuscripts/upload?form%5Bjournal_id%5D%3D27)

Review for this Journal (https://susy.mdpi.com/volunteer/journals/review)

Propose a Special Issue (/journalproposal/sendproposalspecialissue/catalysts)

► Article Menu

Article Menu

MDPI (/)

Academic Editors

Yunfeng Ma

Peng Lu

Xiaole Weng

Recommended Articles

Related Info Link

More by Authors Links

Article Views 905

Citations 7

Table of Contents

- Abstract
- Introduction
- Results and Discussion
- Materials and Methods
- Statistical Analysis
- Conclusions
- Author Contributions
- Funding
- Institutional Review Board Statement
- Data Availability Statement
- Conflicts of Interest
- References

(/toggle_desktop_layout_cookie)

Order Article Reprints (/2073-4344/16/5/468/reprint

Share

Help

Open Access Article

A Visible-Light-Active $TiO_2/Bi_2O_3/g\text{-}C_3N_4$ Heterojunction: Synthesis, Photocatalytic Degradation of Rhodamine B, and Antibacterial Activity

(/toggle_desktop_layout_cookie)
Cite
Discuss in SciProfiles
(https://s
groups/p
utm_sou

by
Lotfi Mouni [1,*] (mailto:l.mouni@univ-bouira.dz) (https://orcid.org/0000-0002-5259-2357),
Oumnia Kasrani [2] (mailto:o.kasrani@univ-bouira.dz) (https://orcid.org/0009-0003-8235-7088),
Zakari Kheznadji [3], **Nasma Bouchelkia** [1,4] (https://orcid.org/0000-0002-6135-2259),
Abdelwahab Rai [1] (mailto:a.rai@univ-bouira.dz) (https://orcid.org/0000-0003-4707-7139),
Gianluca Viscusi [5] (mailto:gviscusi@unisa.it) (https://orcid.org/0000-0002-3458-8901),
Abdelhak Khachay [6] (https://orcid.org/0009-0004-3076-5482), **Farid Ait Merzeg** [7],
Tarek H. Taha [8,*] (mailto:thali@imamu.edu.sa) (https://orcid.org/0000-0002-3607-9529),
Ghareib S. El-Sayyad [8] and
Hamdi Bendif [8] (mailto:hlbendif@imamu.edu.sa) (https://orcid.org/0000-0002-2089-8618)

[1] Laboratoire de Gestion et Valorisation des Ressources Naturelles et Assurance Qualité, Faculté SNVST, Université de Bouira, Bouira 10000, Algeria
[2] Laboratoire de Biotechnologie et Protection des Ecosystèmes Agricoles et Naturels, Faculté SNVST, Université de Bouira, Bouira 10000, Algeria
[3] Laboratory Processes for Materials, Energy, Water and Environment, Faculty of Exact Sciences, University of Bouira, Bouira 10000, Algeria
[4] Centre de Recherche en Technologies Agro-Alimentaires, Route de Targa Ouzemmour, Campus Universitaire, Bejaia 06000, Algeria
[5] Department of Industrial Engineering, University of Salerno, Via Giovanni Paolo II, 132, 84084 Fisciano, Italy
[6] Laboratory of Materials and Environment LME, University of Medea, Medea 26000, Algeria
[7] Technical Platform for Physico-Chemical Analyzes (PTAPC-Bejaia), Targa Ouzemour, Bejaia 06000, Algeria
[8] Department of Biology, College of Science, Imam Mohammad Ibn Saud Islamic University (IMSIU), Riyadh 11623, Saudi Arabia
* Authors to whom correspondence should be addressed.

Catalysts **2026**, *16*(5), 468; **https://doi.org/10.3390/catal16050468 (https://doi.org/10.3390/catal16050468)**

Submission received: 11 April 2026 / Revised: 7 May 2026 / Accepted: 15 May 2026 / Published: 18 May 2026

(This article belongs to the Special Issue **Catalytic Processes in Environmental Applications (/journal/catalysts/special_issues/5T291G0P1V)**)

Download Browse Figures **(https://pub.mdpi-res.com/catalysts/catalysts-16-00468/article_deploy/html/images/catalysts-16-00468-ag.png?1779348207) (https://pub.mdpi-res.com/catalysts/catalysts-16-00468/article_deploy/html/images/catalysts-16-00468-g001.png?1779348187) (https://pub.mdpi-res.com/catalysts/catalysts-16-00468/article_deploy/html/images/catalysts-16-00468-g002.png?1779348192) (https://pub.mdpi-res.com/catalysts/catalysts-16-00468/article_deploy/html/images/catalysts-16-00468-g003.png?1779348196) (https://pub.mdpi-res.com/catalysts/catalysts-16-00468/article_deploy/html/images/catalysts-16-00468-g004.png?1779348198) (https://pub.mdpi-res.com/catalysts/catalysts-16-00468/article_deploy/html/images/catalysts-16-00468-g005.png?1779348200) (https://pub.mdpi-res.com/catalysts/catalysts-16-00468/article_deploy/html/images/catalysts-16-00468-g006.png?1779348201) (https://pub.mdpi-res.com/catalysts/catalysts-16-00468/article_deploy/html/images/catalysts-16-00468-g007.png?1779348204) (https://pub.mdpi-res.com/catalysts/catalysts-16-00468/article_deploy/html/images/catalysts-16-00468-g008.png?1779348205)**

Versions Notes (/2073-4344/16/5/468/notes)

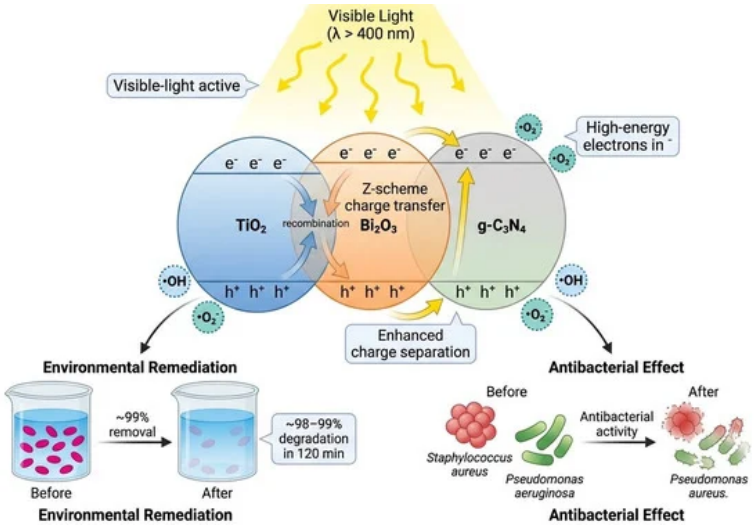
MDPI (/)

Abstract

(/toggle_desktop_layout_cookie)

Ternary heterojunction photocatalysts enhance the separation and transport of photogenerated charge carriers, thereby boosting their redox activity for use in environmental and sustainable energy applications. This study focuses on the synthesis of a $TiO_2/Bi_2O_3/g\text{-}C_3N_4$ heterojunction composite via a ceramic method with TiO_2 loadings of 80%, 85%, and 90% (denoted 80T-BC, 85T-BC, and 90T-BC, respectively) to investigate structure–property–performance relationships in photocatalytic dye degradation. The structural, optical, and morphological properties of the synthesised materials were characterised using X-ray diffraction (XRD), scanning electron microscopy (SEM), and diffuse reflectance UV–Vis spectroscopy (DRS). The photocatalytic performance was evaluated by measuring the degradation of Rhodamine B under visible light irradiation. Under optimised conditions (pH 6, initial RhB concentration of 5 mg/L, and a reaction time of 120 min), a degradation rate of 99% was achieved. Furthermore, the semiconductor demonstrated significant antibacterial activity against both Gram-negative (*Pseudomonas aeruginosa*) and Gram-positive (*Staphylococcus aureus*) bacteria. This study presents a promising strategy for modifying TiO_2-based semiconductors by incorporating different metal oxides. The formation of the resulting heterojunction significantly enhances photocatalytic efficiency, demonstrating strong potential for practical environmental remediation.

Keywords: antibacterial composite (/search?q=antibacterial+composite); $TiO_2/Bi_2O_3/g\text{-}C_3N_4$ (/search?q=TiO2%2FBi2O3%2Fg-C3N4); rhodamine B (/search?q=rhodamine+B); degradation (/search?q=degradation); photocatalytic disinfection (/search?q=photocatalytic+disinfection)



(https://pub.mdpi-res.com/catalysts/catalysts-16-00468/article_deploy/html/images/catalysts-16-00468-ag.png?1779348207)

Graphical Abstract

(/toggle_desktop_layout_cookie)

1. Introduction

The complexity of environmental pollution in hospital settings results from the presence of effluents containing recalcitrant pollutants such as pharmaceuticals, dyes, and microorganisms [**1**,**2**]. In addition, contaminated work surfaces and personal protective equipment, such as medical gowns, can serve as favorable environments for nosocomial pathogens, contributing to healthcare-associated infections (HAIs) [**3**,**4**]. Moreover, biological aerosols released by bacteria in indoor spaces, and the inhalation of airborne pathogenic bacteria that release biological toxins or endotoxins [**5**,**6**,**7**,**8**], as well as exposure to airborne microorganisms often dispersed by ventilation, heating, and air conditioning (VHAC) systems, pose extremely dangerous health risks, causing infections and inflammatory or allergic diseases [**9**,**10**]. Their importance as major reservoirs and vectors of nosocomial infections is highlighted by the high microbial load detected in the air, on surfaces, and on medical devices, including pathogenic microorganisms such as *Staphylococcus aureus*, *Escherichia coli*, and *Pseudomonas aeruginosa* [**11**,**12**,**13**,**14**,**15**]. Eliminating these chemical and biological pollutants becomes challenging using conventional treatment methods, highlighting the need for advanced and multifunctional materials capable of implementing on-demand, environmentally friendly remediation strategies.

Heterogeneous photocatalysis, induced by semiconductor materials, has become the cornerstone of advanced oxidation processes (AOPs), used to remove recalcitrant pollutants, due to its ability to generate reactive oxygen species (ROS), such as hydroxyl radicals (•OH) and superoxide anions ($\bullet O_2^-$), under light radiation. These species can mineralise organic pollutants and inactivate bacteria through oxidative damage that affects DNA and protein synthesis, leading to membrane rupture and cell death [**12**,**16**,**17**,**18**]. Degradation and antibacterial activity are closely linked; however, they are generally studied using different approaches, and very little effort has been made to better understand this relationship by synthesizing a single material with a dual effect.

Among the semiconductor photocatalysts, Titanium dioxide (TiO_2) is the most widely studied thanks to its high activity, chemical stability, and non-toxicity. However, its wide band gap (~3.2 eV for anatase) restricts photoactivation to visible light, accounting for only around 4% of the solar spectrum. Additionally, the rapid recombination of photogenerated electron–hole pairs limits its overall quantum yield [**19**].

In order to exploit visible light, which constitutes the majority of both natural and artificial light, extensive research has been conducted into developing new photocatalysts, such as Bismuth oxide and graphitic carbon nitride. Bismuth oxide (Bi_2O_3) is a promising material for use under visible light due to its narrower band gap (~2.1–2.8 eV), and has shown potential for organic degradation and antibacterial applications [**20**]. However, pure Bi_2O_3 has a major

drawback: poor charge carrier separation. Graphitic carbon nitride (g-C_3N_4), a metal-free polymer highly sensitive to visible light (with a band gap of ~2.7 eV), has attracted considerable interest due to its ease of synthesis, thermal stability, and band positions that are suitable for redox reactions [**21**]. In recent years, graphitic C_3N_4 (g-C_3N_4) has become an excellent photocatalyst for the degradation of organic matter due to thermochemical stability [**22**]. Nevertheless, the rapid recombination of photogenerated carriers in pure g-C_3N_4 hinders its practical application.

Previous studies have explored various strategies for reducing the bandgap energy of titanium dioxide (TiO_2), including n-type and p-type doping [**23**]. Another widely studied approach is to form heterojunctions, i.e., interfaces between two or more n-type or p-type semiconductors [**24**,**25**]. The recent literature has also highlighted the incorporation of semiconductor materials into TiO_2 [**26**]. These composite materials exhibit enhanced optical properties compared to pure TiO_2, due to vacant d orbitals that facilitate electron mobility [**27**,**28**]. The improvement in the photocatalytic activity of these systems is primarily attributed to alterations in the electronic configuration of the dopant metal, arising from charge transfer between the d-electrons of the transition metals and the valence band (VB) of TiO_2 [**29**,**30**]. A powerful strategy for overcoming the inherent limitations of single semiconductors is to construct heterojunction composites. Coupling materials with staggered band alignments creates an interfacial electric field that forces the spatial separation of photogenerated electrons and holes. This dramatically prolongs the lifetime of charge carriers and enhances photocatalytic performance [**31**,**32**]. Binary TiO_2/g-C_3N_4 and Bi_2O_3/g-C_3N_4 heterojunction systems have been widely studied for their ability to degrade pollutants [**33**,**34**]. TiO_2/g-C_3N_4 systems demonstrate enhanced visible-light activity, though they exhibit reduced redox potential in type-II configurations and complex fabrication in Z-scheme designs. Bi_2O_3/g-C_3N_4 composites offer better visible absorption, but they suffer from rapid charge recombination and insufficient active sites. The limitations of incomplete charge separation, narrow light absorption and compromised redox power necessitate the use of ternary heterojunctions, which provide multiple charge transfer pathways and enhanced surface reactivity [**35**].

The TiO_2/Bi_2O_3/g-C_3N_4 system is expected to promote efficient charge separation by facilitating either a step (S)-scheme or a Z-scheme charge transfer mechanism. In this process, less useful charge carriers with weaker redox power recombine at the interface, while the most potent electrons and holes remain in their respective components [**36**]. This achieves exceptional charge separation without compromising high redox potentials [**37**,**38**], making it an excellent design concept for maximizing photocatalytic efficiency for both organic pollutants and biological contaminants degradation and deactivation.

This work focuses on the synthesis and application-oriented testing of a new ternary heterojunction nanocomposite: TiO_2/Bi_2O_3/g-C_3N_4. We hypothesize that optimally integrating these three semiconductors will create an efficient charge transfer pathway, resulting in a material with significantly improved photocatalytic activity in the visible spectrum compared to

binary or single-component materials. The efficiency of the synthetised materials is evaluated using two models: (1) degradation of the toxic, recalcitrant dye Rhodamine B (RhB), which is used as a representative model compound for dye pollutants from various industrial sources, including but not limited to hospital-related discharges, and (2) antibacterial activity against the nosocomial pathogens *Escherichia coli* (*E. coli*) and *Staphylococcus aureus* (*S. aureus*), which represent Gram-negative and Gram-positive bacteria, respectively. Converging materials engineering, photocatalysis, and antimicrobial design, this study provides a comprehensive blueprint for multifunctional nanocomposites that tackle coupled chemical and biological contaminants. Our work paves the way for smarter, safer, and more sustainable infection control and environmental safety protocols in healthcare.

2. Results and Discussion

2.1. Characterization of Synthesized Catalyst

2.1.1. X-Ray Diffraction (XRD) Analysis

Figure 1 displays the X-ray diffraction (XRD) patterns of the synthesized heterojunction nanocomposites.

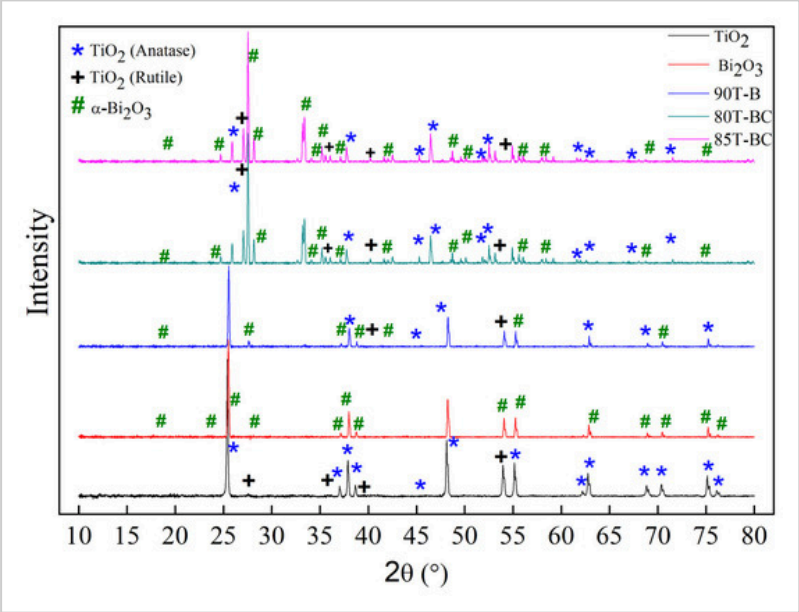


Figure 1. XRD patterns of the synthesized TiO_2-Bi_2O_3-g-C_3N_4 heterojunction nanocomposites.

The diffraction peaks confirm the successful formation of multiphase crystalline structures composed of anatase TiO_2, monoclinic α-Bi_2O_3, and graphitic carbon nitride (g-C_3N_4). For the TiO_2/Bi_2O_3 (90/10) sample calcined at 600 °C, the diffractogram clearly reveals the coexistence of three crystalline phases: anatase TiO_2 (tetragonal) as the major phase, rutile TiO_2 (tetragonal) as a minor phase, and monoclinic α-Bi_2O_3. The characteristic peaks of anatase TiO_2 (JCPDS Card No. 21-1272) are observed at 2θ = 25.3°, 37.8°, 48.1°,

54.0°, and 62.7°, corresponding to the (101), (004), (200), (105), and (204) planes, respectively. The presence of α-Bi_2O_3 (JCPDS Card No. 41-1449) is evidenced by diffraction peaks at 2θ = 27.4°, 33.2°, and 46.3°, attributed to the (120), (200), and (041) planes. For the ternary TiO_2/Bi_2O_3/g-C_3N_4 composites with mass ratios of 8:1:1 and 8.5:0.5:1, the diffractograms exhibit similar diffraction patterns, including the anatase, rutile, and α-Bi_2O_3 phases. A peak at 2θ = 27.53° may be attributed to both g-C_3N_4 and α-Bi_2O_3, suggesting possible peak overlap. However, this reflection is most likely dominated by α-Bi_2O_3, as g-C_3N_4-a non-metallic polymeric semiconductor, typically exhibits poor crystallinity after calcination, and its characteristic (002) interlayer stacking peak near 27.5° may be overshadowed by the more intense diffraction from the crystalline oxide phases. Consequently, while XRD alone cannot definitively confirm the presence of g-C_3N_4, the samples are consistent with ternary TiO_2/α-Bi_2O_3/g-C_3N_4 composites in which anatase remains the predominant phase. The formation of such multiple heterojunctions is particularly advantageous for photocatalytic applications, as it extends light absorption into the visible range through the incorporation of narrower-band-gap semiconductors (Bi_2O_3 and g-C_3N_4) and promotes efficient separation of photogenerated charge carriers at the interfaces between phases. This synergistic effect is expected to reduce electron–hole recombination and enhance the photocatalytic degradation efficiency of organic pollutants in water.

2.1.2. Scanning Electron Microscopy (SEM)

The surface morphology of the synthesized pure TiO_2, Bi_2O_3, 80T-BC, 85T-BC and 90T-B catalysts was examined using Scanning Electron Microscopy (SEM), with the corresponding micrographs presented in **Figure 2**.

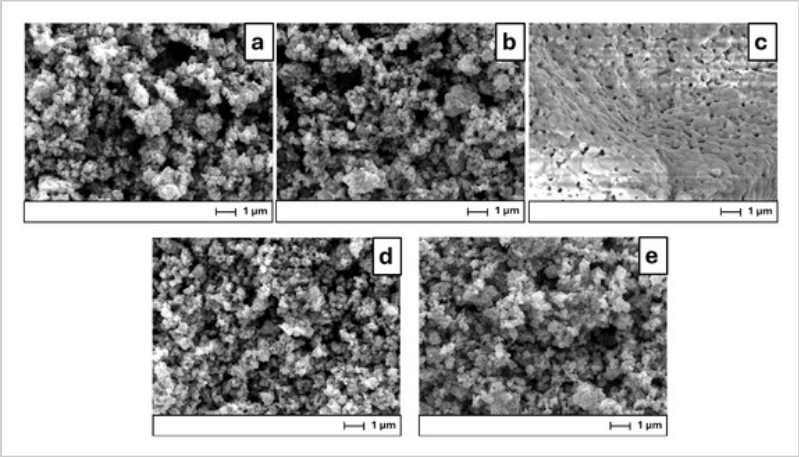


Figure 2. SEM analysis of (**a**) TiO_2, (**b**) 80T-BC, (**c**) Bi_2O_3, (**d**) 85T-BC and (**e**) 90T-B.

The image of pure TiO_2 (**Figure 2**a) reveals particles with an approximately spherical morphology. These particles exhibit a non-uniform size distribution and a propensity for dense agglomeration. This agglomeration is typical of metal oxide nanoparticles synthesised using high-temperature methods. SEM image of Bi_2O_3 shows the presence of agglomerated structures. Following the incorporation of the various components, the morphological

characteristics of the composites did not change significantly. The 80T-BC, 85T-BC, and 90T-B composites (**Figure 2**b,d,e) have a compact structure. The SEM image of the sample 90T-B appears to be more compact than the other two samples 80T-BC and 85T-BC, and exhibits locally denser and brighter areas, showing partial segregation relative to the distribution of Bi_2O_3 particles on the TiO_2. The presence of g-C_3N_4 in the 80T-BC and 85T-BC simples provides better homogeneity and dispersion of phases. This morphology suggests good integration of the components, where dense packing could potentially offer greater surface accessibility, which is beneficial for catalytic applications. Fundamentally, this specific structural arrangement creates an extensive network of interparticle connections. Such intimate contact and interconnection are highly advantageous for photocatalytic applications as they facilitate the efficient transfer of charge carriers between particles. This can potentially reduce electron–hole recombination and improve overall photocatalytic performance.

2.1.3. Diffuse Reflectance Spectroscopy (DRS)

The optical properties and band gap energies of the synthesised TiO_2/Bi_2O_3/g-C_3N_4 ternary heterojunction material were investigated using UV-Vis diffuse reflectance spectroscopy (DRS). **Figure 3** shows the DRS spectra of the heterojunction and its pristine components (TiO_2, Bi_2O_3, and g-C_3N_4) across a wavelength range of 200–800 nm. Pristine TiO_2 exhibits a sharp absorption edge at around 380 nm, which is attributed to its intrinsic band-to-band transition. This UV absorption is characteristic of anatase TiO_2 as a wide-band-gap semiconductor (3.15 eV), with negligible absorption in the visible region (>400 nm). In contrast, Bi_2O_3 shows an absorption edge extending to around 420 nm, confirming its responsiveness to visible light, with an estimated band gap of approximately 2.65 eV. The TiO_2/Bi_2O_3/g-C_3N_4 ternary heterojunction exhibits a composite absorption profile integrating features of its three constituents. Notably, it exhibits significantly greater absorption in the visible spectrum (400–600 nm) than TiO_2, while maintaining strong UV absorption. This enhanced visible-light harvesting capability is attributed to the incorporation of narrow-band-gap components (Bi_2O_3 and g-C_3N_4), which can absorb lower-energy photons. The gradual rather than abrupt absorption edge indicates effective electronic coupling between the components, which is essential for efficient heterojunction performance. The optical band gap energies were determined using the Tauc plot method based on the Kubelka–Munk function (Equation (1)):

$$F(R) = \frac{(1-R)^2}{2R} \quad (1)$$

where R is the reflectance. For indirect band gap semiconductors (TiO_2 and g-C_3N_4), the Tauc relation is expressed as Equation (2):

$$[F(R)h\nu]^{1/2} = A * \left(h\nu - E_g\right) \quad (2)$$

while for direct band gap semiconductors (Bi_2O_3), Equation (3) can be used:

$$[F(R)h\nu]^2 = A * \left(h\nu - E_g\right) \quad (3)$$

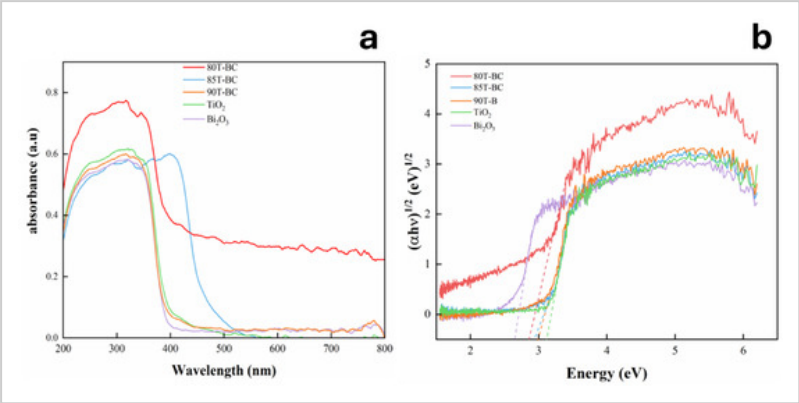


Figure 3. (**a**) UV-vis DRS spectra and (**b**) optical bandgap off 80T-BC, 85T-BC, 90T-B, TiO_2, and Bi_2O_3.

The effective optical band gap of the $TiO_2/Bi_2O_3/g\text{-}C_3N_4$ ternary heterojunction has been estimated to be approximately 2.94 eV. This value lies between the band gaps of its constituents, Bi_2O_3 (2.65 eV) and TiO_2 (3.15 eV), strongly suggesting that each component that is active in visible light contributes synergistically to the composite's extended absorption profile. The reduction in the band gap observed compared to pure TiO_2, and its positioning between the band gaps of Bi_2O_3 and $g\text{-}C_3N_4$ (**Table 1**) implies that an integrated electronic structure has formed rather than a simple physical mixture. Previous studies on similar ternary systems have reported comparable band gap values ranging from 2.2 to 2.9 eV depending on the composition and synthesis method used [**39**,**40**]. The staggered (type II) or staircase alignment of the bands, which usually occurs between these three components, should create an optimal energy landscape at the heterojunction interfaces. Various studies have proposed Z-type or double Z-type charge migration mechanisms for $TiO_2/Bi_2O_3/g\text{-}C_3N_4$ heterojunctions. These mechanisms facilitate the efficient spatial separation of photogenerated charge carriers by directing electrons and holes to migrate in opposite directions across the interfaces [**40**].

Table 1. Optical characteristics of synthesized materials.

2.2. Photocatalytic Activity Study

The photocatalytic performance of the TiO_2, Bi_2O_3, 80T-BC, 85T-BC, and 90T-B heterojunction was evaluated through Rhodamine B (RhB) degradation under visible light xenon lamps BEETRO® (75 W, wavelength = 400 nm). **Figure 4** presents the time-dependent degradation profiles, kinetic analysis, and comparative performance with control samples.

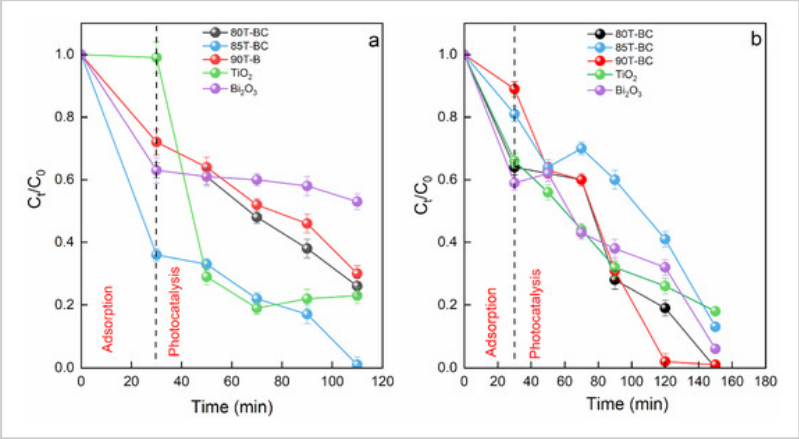


Figure 4. Kinetic degradation of RhB at pH 6 (**a**) and at pH 8 (**b**) under visible light (pH = 6, catalyst loading = 0.5 g/L, $[RhB]_0$ = 5 mg/L).

Figure 4 shows the photocatalytic degradation efficiency of rhodamine B (RhB) on the ternary heterojunction $TiO_2/Bi_2O_3/g\text{-}C_3N_4$ compared to TiO_2 and Bi_2O_3. Upon visible radiation irradiation, the ternary heterojunction exhibited significantly enhanced photocatalytic activity compared to all control samples. Complete RhB degradation (>99%) was achieved within 120 min, whereas TiO_2 reached only 78% in the same time. The degradation kinetics were analyzed using the pseudo-first-order kinetic model (Equation (4)) [**41**] and reported in **Table 2**:

$$\left(\frac{Cads}{Ct}\right) = k * t \quad (4)$$

where k is the apparent rate constant, C_0 is the initial concentration after dark adsorption, and C is the concentration at irradiation time t. The linear plots of $-\ln(C_{ads}/C_t)$ versus irradiation time confirm that RhB photodegradation follows pseudo-first-order kinetics under the experimental conditions.

Table 2. Values of the rate constant (k) for the degradation of the RhB dye 85TB-C, pH = 6.

(/toggle_desktop_layout_cookie)

Table 2 shows the calculated rate constants (k) and correlation coefficients (R^2) for RhB degradation using the synthesised catalysts. The ternary heterojunction 85T-BC showed the highest rate constant among all materials, at k = 0.0338 1/min, which is around 2.0 times higher than pure TiO_2 (0.0165 1/min) and approximately 7.0 times higher than pure Bi_2O_3 (0.0048 1/min). This enhancement of reaction kinetics highlights the synergistic effect of combining TiO_2, Bi_2O_3, and g-C_3N_4 in a single heterojunction architecture. The superior kinetic efficiency of 85T-BC can be attributed to its structural and optical properties. As demonstrated by the DRS analysis, the ternary heterojunction shows an increased absorption range extending into the visible spectrum (up to 421 nm) and an optimised band gap of 2.94 eV, allowing for the effective collection of visible light. Furthermore, the Z-scheme charge transfer mechanism depicted in **Figure 5** ensures that photogenerated electrons and holes are effectively separated by the interfaces of the three components, thereby suppressing the detrimental electron–hole recombination that limits the efficiency of pure TiO_2 and Bi_2O_3.

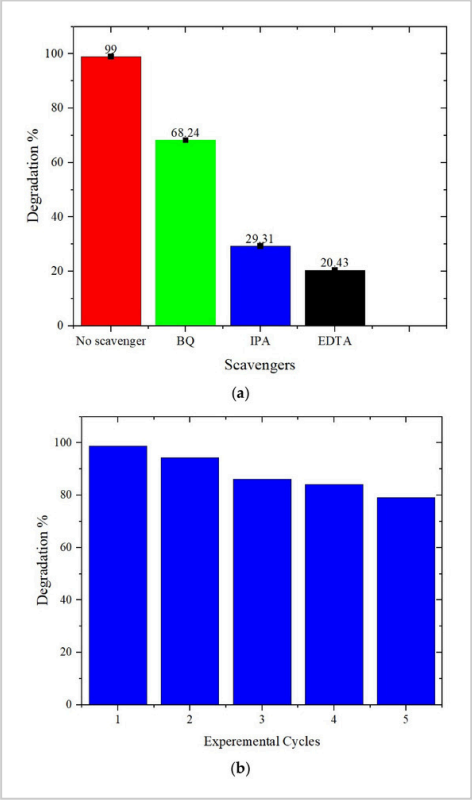


Figure 5. Experiments on free radical scavenging and identification of reactive species for 85T-BC (**a**,**b**) the reusability of the 85T-BC catalyst for RhB degradation after 5 cycles.

MDPI (/toggle_desktop_layout_cookie)

Figure 5a shows the effect of active radicals on the photocatalytic degradation performance of the 85T-BC sample, as determined using selective scavengers. In the absence of any scavenger, the degradation efficiency reached 99%. Adding benzoquinone (BQ), a superoxide radical scavenger, reduced the efficiency to 68.24%, indicating that superoxide radicals play a moderate role in the process.

A more significant decrease was achieved with the addition of isopropanol (IPA), a hydroxyl radical (•OH) scavenger, which lowered the efficiency to 29.31%. The most notable inhibition was caused by EDTA-2Na, a hole scavenger, which lowered the degradation efficiency to just 20.43%. These results indicate that, while all three reactive species participate in the photocatalytic process, holes (h^+) and hydroxyl radicals (•OH) are the most significant active species that contribute to the high degradation efficiency of the $TiO_2/Bi_2O_3/g\text{-}C_3N_4$ sample, whereas superoxide radicals ($•O_2^-$) play a comparatively minor role.

The reusability and photostability of 85T-BC were investigated through consecutive photocatalytic cycles. After each cycle, the catalyst was recovered by centrifugation and rinsed thoroughly with deionised water. It was then dried at 50 °C in ambient air for two hours. As shown in **Figure 5**b, the photocatalytic activity of 85T-BC towards RhB dye degradation under solar irradiation was virtually unaffected during the first two cycles and decreased by only 10% after five cycles.

2.3. Photocatalytic Mechanisms

The $TiO_2/Bi_2O_3/g\text{-}C_3N_4$ composite synthesised in this study exhibits a direct Z-scheme charge transfer mechanism, which enables the efficient spatial separation of photogenerated carriers. When the heterojunction is irradiated with light of equal or greater energy, the three semiconductors simultaneously generate electron–hole pairs (**Figure 6**). The favourable alignment of their band structures means that the electrons generated in the conduction band (CB) of TiO_2 (approximately −0.62 eV vs. ENH) and Bi_2O_3 (approximately +0.33 eV vs. ENH) migrate to the interface, where they recombine with holes generated in the valence band (VB) of $g\text{-}C_3N_4$ (approximately +1.44 eV vs. ENH) [**40**,**42**]. This interfacial recombination process is characteristic of the Z-scheme (**Figure 5**). This is due to the accumulation of electrons in the band gap (BG) of $g\text{-}C_3N_4$, which has a highly negative potential of approximately −1.22 eV vs. ENH and provides strong reducing power. This is ideal for reactions such as hydrogen production or CO_2 reduction. Conversely, holes accumulate in the valence bands of TiO_2 (approximately +2.65 eV vs. ENH) and Bi_2O_3 (approximately +3.13 eV vs. ENH), whose positive potentials provide exceptional oxidizing power for mineralizing organic pollutants or generating reactive oxygen species [**42**]. This orchestration of charge transfer minimizes the harmful recombination of carriers within the same material synergistically, thereby increasing their lifetime and giving the ternary heterojunction photocatalytic superior activity compared to its individual components.

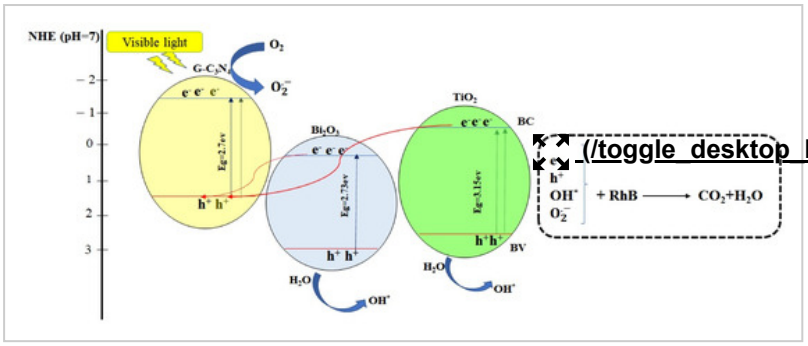


Figure 6. A probable mechanism for the photocatalytic degradation of RhB by the heterojunction 85TB-C under solar irradiation.

The photogenerated electrons and holes migrate to the catalyst surface after excitation. They can engage in redox reactions there with species like O_2 (Equation (5)) and H_2O (Equation (6)) that have been adsorbed from the surrounding media. Highly reactive species, such as hydroxyl radicals (OH•) and superoxide radical anions (O_2•$^-$), are created as a result of this interfacial charge transfer [**31**,**43**]. According to Equations (7) and (8), these radicals start a series of oxidative processes that eventually mineralize the dye pollutant into safe for the environment by producing CO_2 and H_2O [**44**,**45**].

$$e^- + O_2 \rightarrow O_2^{\cdot -} \quad (5)$$

$$h^+ + H_2O \rightarrow OH^{\cdot} + H^+ \qquad h^+ + OH^- \rightarrow OH^{\cdot} \quad (6)$$

$$O_2^{\cdot -} + OH^{\cdot} \rightarrow HOO^{\cdot} \quad (7)$$

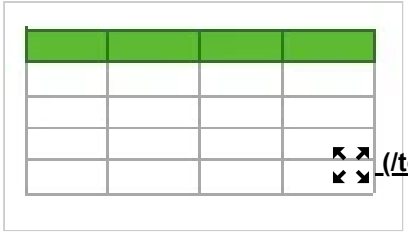
$$HOO^{\cdot} + e^- \rightarrow HO_2^- + h^+ \rightarrow H_2O_2 + h\upsilon \rightarrow 2OH^{\cdot} \quad (8)$$

Photocatalysis decomposition :

$$\begin{cases} O_2^{\cdot -} + RhB \rightarrow CO_2 + H_2O \\ OH^{\cdot} + RhB \rightarrow CO_2 + H_2O \end{cases} \quad (9)$$

Table 3 reports a comparison of the catalytic performance of the designed heterojunctions with literature.

Table 3. Comparative catalytic performance for the degradation of Rhodamine B (RhB).



2.4. Antibacterial Activity

- Against Pseudomonas aeruginosa ATCC 9027

The antibacterial efficacy of the synthesized heterojunction was investigated against the Gram-negative model strain *Pseudomonas aeruginosa* ATCC 9027 using a direct confrontation assay. Bacterial viability was quantified by colony-forming unit (CFU) enumeration, and the corresponding inactivation efficiency (%) was calculated according to Equation (4). The results are summarized in **Table 4**.

Table 4. Effect of the synthesized nanoparticles on *S. aureus* ATCC 6538 and *P. aeruginosa* ATCC 9027 viability. CFU Count and inactivation percentages (%) Inact from cultures obtained after 60 min contact between the bacterium and 85T-BC.



The data demonstrate a pronounced antibacterial activity of the nanomaterial, strongly influenced by the applied concentration, thereby evidencing a clear dose–response relationship. Notably, this activity was significantly enhanced under visible light irradiation (**Figure 7**), highlighting the contribution of photocatalytic processes to the overall antibacterial performance. In contrast, control conditions exhibited substantial bacterial proliferation, particularly in the absence of light, confirming the negligible intrinsic inhibition under dark conditions. Exposure to visible light alone (i.e., in the absence of nanoparticles) induced only a modest reduction in bacterial growth, suggesting a limited photoinhibitory effect.

MDPI (/)

(/toggle_desktop_layout_cookie)

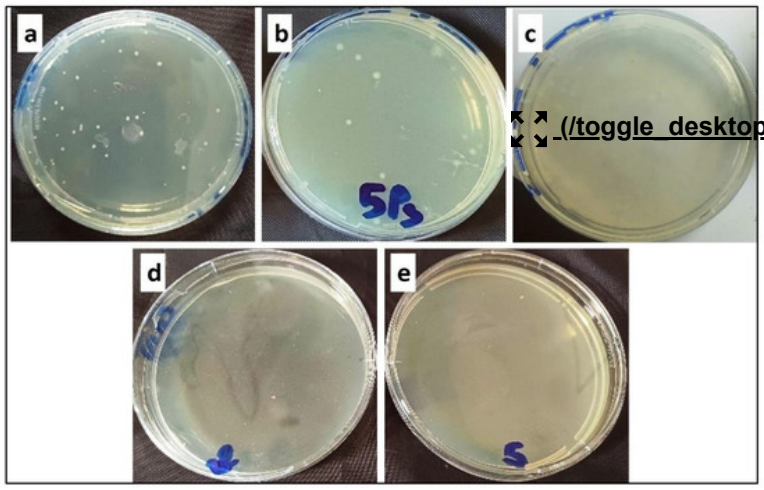


Figure 7. Antibacterial activity of the 85T-BC heterojunction against *Pseudomonas aeruginosa* ATCC 9027 under visible light irradiation, evaluated using the direct confrontation assay. Representative images show the effect of increasing nanoparticle concentrations on bacterial growth: (**a**) control (visible light, no nanoparticles); (**b**) 500 µg/mL; (**c**) 1000 µg/mL; (**d**) 2000 µg/mL; and (**e**) 5000 µg/mL. A progressive reduction in bacterial colonies is observed with increasing concentration, culminating in complete growth inhibition at ≥2000 µg/mL.

At a concentration of 500 µg/mL, the nanomaterial induced a marked reduction in bacterial viability under both illuminated and dark conditions, with a more pronounced effect observed under light irradiation. Increasing the concentration to 1000 µg/mL further enhanced antibacterial activity, indicating a progressive improvement in efficacy. At 2000 µg/mL, near-complete bacterial inactivation was achieved in the dark (99.02% ± 0.10), whereas total inhibition (100% ± 0.00) was observed under visible light exposure. At the highest tested concentration (5000 µg/mL), complete bacterial inactivation was achieved irrespective of illumination conditions.

Collectively, these findings (**Table 4**) demonstrate a synergistic interaction between photocatalytic activation and the intrinsic antimicrobial properties of the 85T-BC heterojunction, culminating in the complete suppression of *P. aeruginosa* at concentrations ≥2000 µg/mL under visible light irradiation.

- Against Staphylococcus aureus ATCC 6538

The antibacterial activity of the synthesized nanoparticles against the Gram-positive strain *Staphylococcus aureus* ATCC 6538 was evaluated by quantifying viable cells through colony-forming unit (CFU) enumeration. The corresponding inactivation efficiency (%) was calculated according to Equation (4), and the results are presented in **Table 4**.

The data reveal a pronounced antibacterial effect that is strongly dependent on nanoparticle concentration, indicating a clear dose–response relationship. In the control groups, a high bacterial load was observed, particularly under dark conditions, confirming the

absence of significant intrinsic inhibition. Conversely, exposure to visible light alone resulted in a noticeable reduction in bacterial counts (**Figure 8**), suggesting a moderate photoinhibitory effect.

(/toggle_desktop_layout_cookie)

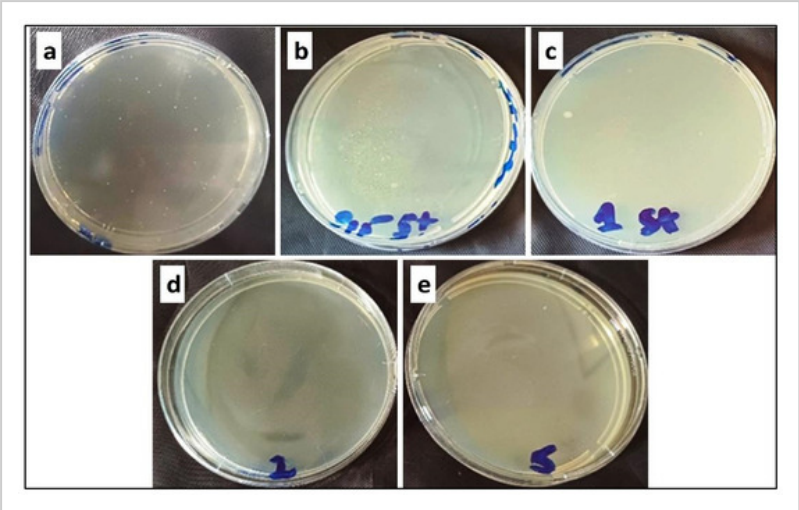


Figure 8. Antibacterial activity of the 85T-BC heterojunction against *Staphylococcus aureus* ATCC 6538 under visible light irradiation, evaluated using the direct confrontation assay. Representative images show the effect of increasing nanoparticle concentrations on bacterial growth: (**a**) control (visible light, no nanoparticles); (**b**) 500 µg/mL; (**c**) 1000 µg/mL; (**d**) 2000 µg/mL; and (**e**) 5000 µg/mL. A progressive reduction in bacterial colonies is observed with increasing concentration, culminating in complete growth inhibition at ≥2000 µg/mL.

At a concentration of 500 µg/mL, nanoparticle treatment significantly reduced bacterial viability under both dark and illuminated conditions. This antibacterial effect increased progressively with concentration, with 1000 µg/mL and 2000 µg/mL leading to near-complete inactivation in the dark (99.74% ± 0.17) and complete inactivation under visible light irradiation (100% ± 0.00). At the highest tested concentration (5000 µg/mL), total bacterial inhibition was achieved irrespective of illumination conditions.

The antibacterial activity of the synthesized heterojunction against the Gram-positive *Staphylococcus aureus* ATCC 6538 and the Gram-negative *Pseudomonas aeruginosa* ATCC 9027 reveals distinct susceptibility patterns, particularly at lower nanoparticle concentrations. Overall, both strains exhibited a concentration-dependent reduction in viability; however, *P. aeruginosa* consistently demonstrated higher resistance compared to *S. aureus* under identical treatment conditions.

At 500 µg/mL under visible light irradiation, *P. aeruginosa* showed slightly higher inactivation efficiency (74.68%) compared to *S. aureus* (68.38%), suggesting an early contribution of photocatalytic activity. In contrast, under dark conditions, a marked difference was observed, with *S. aureus* exhibiting substantially higher susceptibility (75.02%) than *P.*

MDPI (/)
(/toggle_desktop_layout_cookie)

aeruginosa (28.18%), indicating that the intrinsic antibacterial activity of the nanomaterial is less effective against Gram-negative bacteria in the absence of light.

This differential behavior can be attributed to structural differences in the bacterial cell envelope. Gram-negative bacteria possess an additional outer membrane enriched in lipopolysaccharides, which acts as a permeability barrier and limits nanoparticle penetration and interaction. Conversely, the thicker but more permeable peptidoglycan layer in Gram-positive bacteria facilitates greater interaction with the nanomaterial, enhancing its antibacterial effect under non-irradiated conditions [**49**,**50**].

At intermediate concentrations (1000 µg/mL), the antibacterial activity increased substantially for both strains, with reduced differences between them, suggesting that higher nanoparticle doses can partially overcome the protective barrier of Gram-negative bacteria. At concentrations ≥2000 µg/mL, both bacterial strains exhibited near-complete or complete inactivation regardless of illumination conditions, indicating that the combined effects of nanoparticle concentration and photocatalytic activation are sufficient to induce total bacterial eradication.

Under visible light irradiation, the differences between Gram-positive and Gram-negative bacteria became less pronounced across all concentrations, highlighting the dominant role of photocatalytically generated reactive oxygen species (ROS) in bacterial inactivation mediated by TiO_2, Bi_2O_3, and g-C_3N_4 under light activation. These ROS, including hydroxyl radicals and superoxide anions, are known to induce oxidative stress by damaging critical cellular components. Specifically, they disrupt bacterial cell envelopes and compromise membrane integrity, while also targeting intracellular biomolecules such as proteins and nucleic acids, ultimately leading to irreversible cell death [**51**,**52**,**53**,**54**].

Recent studies have consistently demonstrated the remarkable antibacterial potential of TiO_2-based heterojunctions incorporating Bi_2O_3 and g-C_3N_4, highlighting their promise for advanced biomedical and environmental applications [**55**,**56**]. These composite systems exhibit enhanced photocatalytic and antibacterial performance under visible light irradiation, which is primarily attributed to improved charge carrier separation, increased specific surface area, and favorable heterojunction architecture.

The antibacterial efficiencies observed in the present study are consistent with previously reported TiO_2-based systems. For instance, Luthfiah et al. [**57**] reported inactivation rates of 98.69% for *Staphylococcus aureus* and 97.44% for *Pseudomonas aeruginosa*, as determined by optical density and dilution assays. Similarly, Li et al. [**58**] demonstrated that visible LED irradiation induces significant oxidative damage to the cell membrane of *S. aureus*, further supporting the role of ROS-mediated mechanisms in photocatalytic antibacterial activity.

3. Materials and Methods

3.1. Biological Material

In this study, two bacterial strains were used, including a Gram-positive bacterium, such as *Staphylococcus aureus* ATCC 6538, and a Gram-negative bacterium, *Pseudomonas aeruginosa* ATCC 9027 (ATCC: American Type Culture Collection).

3.2. Chemicals

The chemical reagents and solvents used in this study were analytical grade bismuth (III) oxide (Bi_2O_3, 99.9%, MW = 465.96 g mol^{-1}), titanium oxide (TiO_2, 99.5%, MW = 79.89 g mol^{-1}), Urea ($CO(NH_2)_2$), Rhodamine B (479.02 g mol^{-1}), NaOH (39.99 g mol^{-1}), HCl (36.47 g mol^{-1}), which were obtained from Sigma Aldrich® (Darmstadt, Germany). All reagents were used without further purification, and all solutions were prepared with locally produced deionized water.

3.3. Synthesis of $TiO_2/Bi_2O_3/g\text{-}C_3N_4$ Catalyst

In this study, the heterojunctions $TiO_2/Bi_2O_3/g\text{-}C_3N_4$ were synthesized through a common solid-state reaction route [**25**]. Bismuth oxide (Bi_2O_3) powder was first homogenized by grinding in a ceramic mortar to ensure uniform particle size distribution. The ground Bi_2O_3 was subsequently calcined in a muffle furnace (Nabertherm®, Lilienthal, Germany) at 500 °C for 2 h. Separately, urea was subjected to thermal polymerization by calcination at 550 °C for 2 h, leading to the formation of graphitic carbon nitride ($g\text{-}C_3N_4$). For the preparation of the composite material, $(90\text{-}x)TiO_2/10Bi_2O_3/x\ g\text{-}C_3N_4$, the appropriate amounts of the starting materials were mixed and thoroughly ground in an agate (or ceramic) mortar for 2 h [**25**]. The resulting mixture was then calcined at 600 °C for 6 h to form the final product. A series of samples was prepared with a fixed Bi_2O_3 content of 10 wt.% and varying TiO_2 concentrations. These composites are labeled as 80T-BC, 85T-BC, and 90T-B, where T stands for TiO_2, B for Bi_2O_3 and C for $g\text{-}C_3N_4$ while the number indicates the weight percentage of TiO_2 (i.e., y = 80%, 85%, and 90%, respectively).

3.4. Photodegradation of Rhodamine B Dye

The photocatalytic efficiency of the catalysts 80T-BC, 85T-BC, 90T-B, TiO_2, and Bi_2O_3 was evaluated through the degradation of Rhodamine B (RhB) dye in aqueous solution under visible light irradiation xenon lamps BEETRO® (75 W, wavelength = 400 nm). A catalyst loading (0.5 g) was dispersed in a 100 mL solution containing RhB dye at a concentration of 5 mg/L and pH = 6. Before the light irradiation, the suspension of the catalyst in the RhB solution was first stirred for 30 min in darkness to achieve adsorption–desorption equilibrium. Then the solution was irradiated under the light source with constant stirring. Samples of 2 mL were taken every 15 min, and absorbances were measured at 665 nm. The degradation efficiency (R) was determined using Equation (10).

$$\mathrm{R}\ (\%) = \frac{c_0 - c_t}{c_0} \times 100 = \frac{A_0 - A_t}{A_0} \times 100 \quad (10)$$

(/toggle_desktop_layout_cookie)

where C_0 and A_0 represent the concentration and the absorbance of dye after the adsorption and desorption equilibrium, and C_t and A_t represent the concentration and the absorbance after a given time of degradation. Therefore, examining the degradation kinetics is essential, as it provides critical insights into the efficiency and rate of the process. To determine the rate constant, the Langmuir-Hinshelwood model (Equation (11)) was applied, which simplifies to a pseudo-first-order kinetic model (Equation (12)):

$$r = \frac{-dC_t}{dt} = \frac{kKC_t}{1 + KC_t} \quad (11)$$

$$C_t = C_{ads} * e^{-k't} \quad (12)$$

where k is the photocatalytic rate constant [mg/(min·L)], *K* is the adsorption equilibrium constant [L/mg], and *k′* is the pseudo-first-order rate constant [1/min].

The contributions of superoxide radicals ($\bullet O_2^-$), holes (h^+) and hydroxyl radicals (•OH) to the photocatalytic mechanism were examined using targeted radical inhibitors. Benzoquinone (BQ) was used to quench superoxide radicals, sodium ethylenediaminetetraacetate (EDTA-2Na) to scavenge holes, and isopropanol (IPA) to inhibit hydroxyl radicals. The inhibitory experiments were performed under conditions similar to those of the photocatalytic tests, with the exception of the addition of the respective inhibitors to the solution.

3.5. The Characterization of Synthesized Catalysts

A series of characterization techniques was used to determine the structural, optical, and electronic properties of the synthesized 90-xTiO_2/xBi_2O_3/10 g-C_3N_4 heterojunction at different ratios and the raw materials Bi_2O_3, TiO_2.

The crystalline phases and crystallographic structure were determined by X-ray diffraction (XRD) using a PANALYTICAL EMPYREAN® (Almelo, The Netherlands) diffractometer with CuKα radiation, scanning a 2θ range from 20° to 80°.

The surface morphology and particle shape were analyzed using a scanning electron microscope (SEM, JEOL Ltd., Tokyo, Japan) at different magnifications.

The optical properties, namely the estimation of the band gap, were studied by diffuse reflectance spectroscopy (DRS) between 200 and 800 nm using an Evolution 220 UV-Vis spectrometer (Thermo Fisher Scientific, Madison, WI, USA).

3.6. Antibacterial Activity

The antibacterial activity of the synthesized heterojunction nanoparticles was evaluated using a quantitative liquid-phase contact (confrontation) assay against representative Gram-

negative and Gram-positive bacteria, namely *Pseudomonas aeruginosa* (ATCC 9027) and *Staphylococcus aureus* (ATCC 6538), respectively.

3.6.1. Preparation of Nanoparticle Suspensions

(/toggle_desktop_layout_cookie)

Stock suspensions of nanoparticles were prepared at concentrations of 500, 1000, 2000, and 5000 μg·mL^{-1} by dispersing the appropriate mass of nanoparticle powder in sterile physiological saline (0.9% NaCl). Suspensions were magnetically stirred until complete homogenization and subsequently adjusted to pH 7.0 ± 0.1.

3.6.2. Preparation of Bacterial Inocula

Fresh bacterial cultures were grown overnight and adjusted to an optical density of OD_{600} = 0.08–0.10, corresponding to approximately 10^8 CFU·mL^{-1}. The suspensions were then serially diluted in sterile saline to obtain a working inoculum of ~10^5 CFU·mL^{-1}.

3.6.3. Antibacterial Assay Conditions

For each experimental condition, 1 mL of the bacterial suspension (~10^5 CFU·mL^{-1}) was mixed with 9 mL of nanoparticle suspension at the desired concentration. The mixtures were incubated for 60 min under both visible light irradiation and dark conditions. A total of 10 experimental conditions were evaluated for each bacterial strain:

- T1: control under visible light (bacteria + sterile saline solution);
- T2: control in dark (bacteria + sterile saline solution);
- T3: 500 μg/mL nanoparticles under visible light;
- T4: 500 μg/mL nanoparticles in dark;
- T5: 1000 μg/mL nanoparticles under visible light;
- T6: 1000 μg/mL nanoparticles in dark;
- T7: 2000 μg/mL nanoparticles under visible light;
- T8: 2000 μg/mL nanoparticles in dark;
- T9: 5000 μg/mL nanoparticles under visible light;
- T10: 5000 μg/mL nanoparticles in dark.

All experiments were performed in duplicate.

3.6.4. Enumeration of Viable Bacteria

Following incubation, aliquots (100 μL) from each treatment were spread onto nutrient agar plates and incubated at 37 °C for 18–24 h. Viable bacterial cells were quantified by counting colony-forming units (CFU).

3.6.5. Calculation of Antibacterial Activity

The antibacterial efficiency was expressed as the percentage of bacterial inactivation (%), calculated by comparing the number of viable cells after treatment (N) to that of the untreated control (N_0), according to Equation (13):

$$\text{Bacterial inactivation } (\%) = \frac{N_0 - N}{N_0} \times 100 \quad (13)$$

where N_0 is the CFU count of the control sample; N is the CFU count after treatment.

4. Statistical Analysis

Data from the microbiological analysis are presented as mean ± standard deviation (SD). Statistical differences among treatment groups were evaluated using one-way analysis of variance (ANOVA). When significant effects were detected, Tukey's honestly significant difference (HSD) test was applied for post hoc multiple comparisons to identify statistically distinct groups. Differences were considered statistically significant at $p < 0.05$. All analyses were performed using the R statistical environment (R Foundation for Statistical Computing, Vienna, Austria).

5. Conclusions

This study successfully produced a novel ternary n-p heterojunction photocatalyst, TiO_2-Bi_2O_3-g-C_3N_4, using a ceramic technique. The prepared materials were thoroughly characterised and their photocatalytic effectiveness evaluated by study of the degradation of a cationic dye model pollutant (RhB). Structural analysis revealed that pure crystalline phases with a uniform distribution of spherical grains formed when Bi_2O_3 and g-C_3N_4 were added to the TiO_2 matrix.

Optical analysis using DRS showed that the ternary heterojunction has an extended absorption edge into the visible spectrum (up to ~421 nm) and an optimised band gap of 2.94 eV, allowing for the efficient harvesting of visible light. Near-complete degradation (>99%) was achieved within 110 min, with a rate constant (k = 0.0338 1/min) about 2.0 times higher than that of pure TiO_2 and around 7.0 times higher than that of pure Bi_2O_3.

Additionally, the composite exhibited notable antibacterial activity, particularly against *S. aureus*, achieving nearly complete eradication of viable cells at concentrations as low as 0.5 mg/mL. These results suggest that the synthesised composite could be an effective, multifunctional agent for cleaning contaminated water and disinfecting surfaces in hospital environments.

Author Contributions

Conceptualization, O.K., L.M. and Z.K.; software, A.R., O.K. and F.A.M.; validation, L.M., A.R. and N.B.; formal analysis, O.K., F.A.M. and G.V.; investigation, L.M., A.K., O.K. and Z.K.; resources, H.B.; writing—original draft preparation, A.K., L.M., O.K., A.R. and Z.K.; writing—review and editing, G.S.E.-S.,T.H.T. and H.B., L.M., N.B. and G.V.; supervision, A.R. and

L.M.: funding acquisition, T.H.T. and H.B.; project administration, G.S.E.-S. and H.B. All authors have read and agreed to the published version of the manuscript.

(/toggle_desktop_layout_cookie)

Funding

This work was supported and funded by the Deanship of Scientific Research at Imam Mohammad Ibn Saud Islamic University (IMSIU) (grant number IMSIU-DDRSP2602).

Institutional Review Board Statement

Not applicable.

Data Availability Statement

Data supporting this project are available from the corresponding author upon reasonable request.

Conflicts of Interest

The authors declare that they have no known competing financial interests or personal relationships.

References

1. Kovalova, L.; Siegrist, H.; Singer, H.; Wittmer, A.; McArdell, C.S. Hospital wastewater treatment by membrane bioreactor: Performance and efficiency for organic micropollutant elimination. *Environ. Sci. Technol.* **2012**, *46*, 1536–1545. [**Google Scholar (https://scholar.google.com/scholar_lookup?title=Hospital+wastewater+treatment+by+membrane+bioreactor:+Performance+and+efficiency+for+organic+micropollutant+elimination&author=Kovalova,+L.&author=Siegrist,+H.&author=Singer,+H.&author=Wittmer,+A.&author=McArdell,+C.S.&publication_year=2012&journal=Environ.+Sci.+Technol.&volume=46&pages=1536%E2%80%931545&doi=10.1021/es203495d)**] [**CrossRef (https://doi.org/10.1021/es203495d)**] [**Scilit (https://www.scilit.com/publications/6705a737cb82cd5bc0915c9c1624a735)**]

2. Verlicchi, P.; Al Aukidy, M.; Galletti, A.; Petrovic, M.; Barceló, D. Hospital effluent: Investigation of the concentrations and distribution of pharmaceuticals and environmental risk assessment. *Sci. Total Environ.* **2012**, *430*, 109–118. [**Google Scholar (https://scholar.google.com/scholar_lookup?title=Hospital+effluent:+Investigation+of+the+concentrations+and+distribution+of+pharmaceuticals+and+environmental+risk+assessment&author=Verlicchi,+P.&author=Al+Aukidy,+M.&author=Galletti,+A.&author=Petrovic,+M.&author=Barcel%C3%B3,+D.&publication_year=2012&journal=Sci.+Total+Environ.&volume=430&pages=109%E2%80%93118&doi=10.1016/j.scitotenv.2012.04.055)**] [**CrossRef (https://doi.org/10.1016/j.scitotenv.2012.04.055)**] [**Scilit (https://www.scilit.com/publications/9c4c8744ddb482adba9a5596a17bd526)**]

3. Sartelli, M.; Marini, C.P.; McNelis, J.; Coccolini, F.; Rizzo, C.; Labricciosa, F.M.; Petrone, P. Preventing and controlling healthcare-associated infections: The first principle of every antimicrobial stewardship program in hospital settings. *Antibiotics* **2024**, *13*, 896. [**Google Scholar (https://scholar.google.com/scholar_lookup?title=Preventing+and+controlling+healthcare-associated+infections:+The+first+principle+of+every+antimicrobial+stewardship+program+in+hospital+settings&author=Sartelli,+M.&author=Marini,+C.P.&author=McNelis,+J.&author=Coccolini,+F.&author=Rizzo,+C.&author=Labricciosa,+F.M.&author=Petrone,+P.&publication_year=2024&journal=Antibiotics&volume=13&pages=896&doi=10.3390/antibiotics13090896)**] [**CrossRef (https://doi.org/10.3390/antibiotics13090896)**] [**Scilit (https://www.scilit.com/publications/95bbb823c976829c6403ddd29b432dbc)**]

4. Li, Y.; Fan, Y.; Jiang, L.; Wang, H. Aerosol and environmental surface monitoring for SARS-CoV-2 RNA in a designated hospital for severe COVID-19 patients. *Epidemiol. Infect.* **2020**, *148*, e154. [**Google Scholar (https://scholar.google.com/scholar_lookup?title=Aerosol+and+environmental+surface+monitoring+for+SARS-CoV-2+RNA+in+a+designated+hospital+for+severe+COVID-19+patients&author=Li,+Y.&author=Fan,+Y.&author=Jiang,+L.&author=Wang,+H.&publication_year=2020&journal=Epidemiol.+Infect.&volume=148&pages=e154&doi=10.1017/S0950268820001570&pmid=32660668)**] [**CrossRef (https://doi.org/10.1017/S0950268820001570)**] [**Scilit (https://www.scilit.com/publications/8a282ef0afed53fa380375aa1faebefb)**] [**PubMed (https://www.ncbi.nlm.nih.gov/pubmed/32660668)**]

5. Al-Shaarani, A.A.; Pecoraro, L. A review of pathogenic airborne fungi and bacteria: Unveiling occurrence, sources, and profound human health implication. *Front. Microbiol.* **2024**, *15*, 1428415. [**Google Scholar (https://scholar.google.com/scholar_lookup?title=A+review+of+pathogenic+airborne+fungi+and+bacteria:+Unveiling+occurrence,+sources,+and+profound+human+health+implication&author=Al-Shaarani,+A.A.&author=Pecoraro,+L.&publication_year=2024&journal=Front.+Microbiol.&volume=15&pages=1428415&doi=10.3389/fmicb.2024.1428415&pmid=39364169)**] [**CrossRef (https://doi.org/10.3389/fmicb.2024.1428415)**] [**Scilit (https://www.scilit.com/publications/5b11e7db60a5ad513206df859707fa62)**] [**PubMed (https://www.ncbi.nlm.nih.gov/pubmed/39364169)**]

6. Salari, M.; Ardakani, M.A.; Nasab, H.; Madadizadeh, F.; Teimouri, F.; Ehrampoush, M.H.; Soltaniyanzadeh, Z.; Sadeh, M.; Eslami, G.; Ebrahimi, A.A. Evaluation of bacterial bioaerosols and their relationship with environmental factors in the air of the wastewater treatment plant of industrial. *Sci. Rep.* **2025**, *15*, 44827. [**Google Scholar (https://scholar.google.com/scholar_lookup?title=Evaluation+of+bacterial+bioaerosols+and+their+relationship+with+environmental+factors+in+the+air+of+the+wastewater+treatment+plant+of+industrial&author=Salari,+M.&author=Ardakani,+M.A.&author=Nasab,+H.&author=Madadizadeh,+F.&author=Teimouri,+F.&author=Ehrampoush,+M.H.&author=Soltaniyanzadeh,+Z.&author=Sadeh,+M.&author=Eslami,+G.&author=Ebrahimi,+A.A.&publication_year=2025&journal=Sci.+Rep.&volume=15&pages=44827&doi=10.1038/s41598-025-28692-1&pmid=41462540)**] [**CrossRef (https://doi.org/10.1038/s41598-025-28692-1)**] [**Scilit (https://www.scilit.com/publications/6a83d6dd4a32afb2d690b8f54f551ce5)**] [**PubMed (https://www.ncbi.nlm.nih.gov/pubmed/41462540)**]

7. Amin, H.; Santl-Temkiv, T.; Cramer, C.; Finster, K.; Real, F.G.; Gislason, T.; Holm, M.; Janson, C.; Jogi, N.O.; Jogi, R. Indoor airborne microbiome and endotoxin: Meteorological events and occupant characteristics are important determinants. *Environ. Sci. Technol.* **2023**, *57*, 11750–11766. [**Google Scholar (https://scholar.google.com/scholar_lookup?title=Indoor+airborne+microbiome+and+endotoxin:+Meteorological+events+and+occupant+characteristics+are+important+determinants&author=Amin,+H.&author=Santl-Temkiv,+T.&author=Cramer,+C.&author=Finster,+K.&author=Real,+F.G.&author=Gislason,+T.&author=Holm,+M.&author=Janson,+C.&author=Jogi,+N.O.&author=Jogi,+R.&publication_year=2023&journal=Environ.+Sci.+Technol.&volume=57&pages=11750%E2%80%9311766&doi=10.1021/acs.est.3c01616)**] [**CrossRef (https://doi.org/10.1021/acs.est.3c01616)**] [**Scilit (https://www.scilit.com/publications/2b76772bbc3b56592ae97fa399d90db7)**]

8. Passi, A.; Nagendra, S.S.; Maiya, M. Characteristics of indoor air quality in underground metro stations: A critical review. *Build. Environ.* **2021**, *198*, 107907. [**Google Scholar (https://scholar.google.com/scholar_lookup?title=Characteristics+of+indoor+air+quality+in+underground+metro+stations:+A+critical+review&author=Passi,+A.&author=Nagendra,+S.S.&author=Maiya,+M.&publication_year=2021&journal=Build.+Environ.&volume=198&pages=107907&doi=10.1016/j.buildenv.2021.107907)**] [**CrossRef (https://doi.org/10.1016/j.buildenv.2021.107907)**] [**Scilit (https://www.scilit.com/publications/22b7c7fe5b961101fe95c55e5017ceee)**]

9. Lydeamore, M.J.; Mitchell, B.G.; Bucknall, T.; Cheng, A.C.; Russo, P.L.; Stewardson, A.J. Burden of five healthcare associated infections in Australia. *Antimicrob. Resist. Infect. Control* **2022**, *11*, 69. [**Google Scholar (https://scholar.google.com/scholar_lookup?title=Burden+of+five+healthcare+associated+infections+in+Australia&author=Lydeamore,+M.J.&author=Mitchell,+B.G.&author=Bucknall,+T.&author=Cheng,+A.C.&author=Russo,+P.L.&author=Stewardson,+A.J.&publication_year=2022&journal=Antimicrob.+Resist.+Infect.+Control&volume=11&pages=69&doi=10.1186/s13756-022-01109-8)**] [**CrossRef (https://doi.org/10.1186/s13756-022-01109-8)**] [**Scilit (https://www.scilit.com/publications/ac760d714da68ba7373c3bd0baefeaa8)**]

10. Li, X.; Kevin, K.; Lam, W.K.; Ooi, A.; Zachreson, C.; Geard, N.; Tsigaras, L.; Bates, S.; McGain, F.; Morawska, L. Mitigating Airborne Infection Transmission in the Common Area of Inpatient Wards—A Case Study. *Fluids* **2025**, *10*, 267. [**Google Scholar (https://scholar.google.com/scholar_lookup?title=Mitigating+Airborne+Infection+Transmission+in+the+Common+Area+of+Inpatient+Wards%E2%80%94A+Case+Study&author=Li,+X.&author=Kevin,+K.&author=Lam,+W.K.&author=Ooi,+A.&author=Zachreson,+C.&author=Geard,+N.&author=Tsigaras,+L.&author=Bates,+S.&author=McGain,+F.&author=Morawska,+L.&publication_year=2025&journal=Fluids&volume=10&pages=267&doi=10.3390/fluids10100267)**] [**CrossRef (https://doi.org/10.3390/fluids10100267)**] [**Scilit (https://www.scilit.com/publications/586423f966265ccfec5da84eb26ced4d)**]

11. Sandu, A.M.; Chifiriuc, M.C.; Vrancianu, C.O.; Cristian, R.-E.; Alistar, C.F.; Constantin, M.; Paun, M.; Alistar, A.; Popa, L.G.; Popa, M.I. Healthcare-associated infections: The role of microbial and environmental factors in infection control—A narrative review. *Infect. Dis. Ther.* **2025**, *14*, 933–971. [**Google Scholar (https://scholar.google.com/scholar_lookup?title=Healthcare-associated+infections:+The+role+of+microbial+and+environmental+factors+in+infection+control%E2%80%94A+narrative+review&author=Sandu,+A.M.&author=Chifiriuc,+M.C.&author=Vrancianu,+C.O.&author=Cristian,+R.-E.&author=Alistar,+C.F.&author=Constantin,+M.&author=Paun,+M.&author=Alistar,+A.&author=Popa,+L.G.&author=Popa,+M.I.&publication_year=2025&journal=Infect.+Dis.+Ther.&volume=14&pages=933%E2%80%93971&doi=10.1007/s40121-025-01143-0)**] [**CrossRef (https://doi.org/10.1007/s40121-025-01143-0)**] [**Scilit (https://www.scilit.com/publications/c5c55d1ac7861f4abe342ba0860d4e13)**]

12. Rokicka-Konieczna, P.; Morawski, A.W. Photocatalytic bacterial destruction and mineralization by TiO_2-based photocatalysts: A mini review. *Molecules* **2024**, *29*, 2221. [**Google Scholar (https://scholar.google.com/scholar_lookup?title=Photocatalytic+bacterial+destruction+and+mineralization+by+TiO2-based+photocatalysts:+A+mini+review&author=Rokicka-Konieczna,+P.&author=Morawski,+A.W.&publication_year=2024&journal=Molecules&volume=29&pages=2221&doi=10.3390/molecules29102221)**] [**CrossRef (https://doi.org/10.3390/molecules29102221)**] [**Scilit (https://www.scilit.com/publications/98253c938b7f4f6720c508d3cad91b59)**]

13. Hiwar, W.; King, M.F.; Shuweihdi, F.; Fletcher, L.A.; Dancer, S.J.; Noakes, C.J. What is the relationship between indoor air quality parameters and airborne microorganisms in hospital environments? A systematic review and meta-analysis. *Indoor Air* **2021**, *31*, 1308–1322. [**Google Scholar (https://scholar.google.com/scholar_lookup?title=What+is+the+relationship+between+indoor+air+quality+parameters+and+airborne+microorganisms+in+hospital+environments?+A+systematic+review+and+meta-analysis&author=Hiwar,+W.&author=King,+M.F.&author=Shuweihdi,+F.&author=Fletcher,+L.A.&author=Dancer,+S.J.&author=Noakes,+C.J.&publication_year=2021&journal=Indoor+Air&volume=31&pages=1308%E2%80%931322&doi=10.1111/ina.12846)**] [**CrossRef (https://doi.org/10.1111/ina.12846)**] [**Scilit (https://www.scilit.com/publications/8155766797f6facaebf98338fe48534a)**]

14. Belay, M.M.; Ambelu, A.; Mekonen, S.; Karbana, G.; Yemane, B. Investigating microbial contamination of indoor air, environmental surfaces, and medical equipment in a Southwestern Ethiopia Hospital. *Environ. Health Insights* **2024**, *18*, 11786302241266052. [**Google Scholar (https://scholar.google.com/scholar_lookup?title=Investigating+microbial+contamination+of+indoor+air,+environmental+surfaces,+and+medical+equipment+in+a+Southwestern+Ethiopia+Hospital&author=Belay,+M.M.&author=Ambelu,+A.&author=Mekonen,+S.&author=Karbana,+G.&author=Yemane,+B.&publication_year=2024&journal=Environ.+Health+Insights&volume=18&pages=11786302241266052&doi=10.1177/11786302241266052&pmid=39055115)**] [**CrossRef (https://doi.org/10.1177/11786302241266052)**] [**Scilit (https://www.scilit.com/publications/7da46874abbc6bf51ba02fe94450385d)**] [**PubMed (https://www.ncbi.nlm.nih.gov/pubmed/39055115)**]

15. Cappelli, G.; Rapi, I.; Dugheri, S.; Fanfani, N.; Traversini, V.; Baldassarre, A.; Korelidou, A.; Mersel, M.-A.; Baravelli, F.; Louka, M. Managing and monitoring indoor air quality and surface decontamination in healthcare environments. *Arh. Hig. Rada Toksikol.* **2025**, *76*, 222–241. [**Google Scholar (https://scholar.google.com/scholar_lookup?title=Managing+and+monitoring+indoor+air+quality+and+surface+decontamination+in+healthcare+environments&author=Cappelli,+G.&author=Rapi,+I.&author=Dugheri,+S.&author=Fanfani,+N.&author=Traversini,+V.&author=Baldassarre,+A.&author=Korelidou,+A.&author=Mersel,+M.-A.&author=Baravelli,+F.&author=Louka,+M.&publication_year=2025&journal=Arh.+Hig.+Rada+Toksikol.&volume=76&pages=222%E2%80%93241&doi=10.2478/aiht-2025-76-4013&pmid=41491979)**] [**CrossRef (https://doi.org/10.2478/aiht-2025-76-4013)**] [**Scilit (https://www.scilit.com/publications/addd251836b2c742458d0463525a23e4)**] [**PubMed (https://www.ncbi.nlm.nih.gov/pubmed/41491979)**]

16. Foster, H.A.; Ditta, I.B.; Varghese, S.; Steele, A. Photocatalytic disinfection using titanium dioxide: Spectrum and mechanism of antimicrobial activity. *Appl. Microbiol. Biotechnol.* **2011**, *90*, 1847–1868. [**Google Scholar (https://scholar.google.com/scholar_lookup?title=Photocatalytic+disinfection+using+titanium+dioxide:+Spectrum+and+mechanism+of+antimicrobial+activity&author=Foster,+H.A.&author=Ditta,+I.B.&author=Varghese,+S.&author=Steele,+A.&publication_year=2011&journal=Appl.+Microbiol.+Biotechnol.&volume=90&pages=1847%E2%80%931868&doi=10.1007/s00253-011-3213-7)**] [**CrossRef (https://doi.org/10.1007/s00253-011-3213-7)**] [**Scilit (https://www.scilit.com/publications/609bff2b3ebd594dfd82b5f796835873)**]

17. Fujishima, A.; Zhang, X.; Tryk, D.A. TiO_2 photocatalysis and related surface phenomena. *Surf. Sci. Rep.* **2008**, *63*, 515–582. [**Google Scholar (https://scholar.google.com/scholar_lookup?title=TiO2+photocatalysis+and+related+surface+phenomena&author=Fujishima,+A.&author=Zhang,+X.&author=Tryk,+D.A.&publication_year=2008&journal=Surf.+Sci.+Rep.&volume=63&pages=515%E2%80%93582&doi=10.1016/j.surfrep.2008.10.001)**] [**CrossRef (https://doi.org/10.1016/j.surfrep.2008.10.001)**] [**Scilit (https://www.scilit.com/publications/9be7003e30a23497fbad96d7a4c8b0d7)**]

18. Lazić, V.; Nikšić, V.; Nedeljković, J.M. Application of TiO_2 in photocatalytic bacterial inactivation. *Int. J. Mol. Sci.* **2025**, *26*, 10593. [**Google Scholar (https://scholar.google.com/scholar_lookup?title=Application+of+TiO2+in+photocatalytic+bacterial+inactivation&author=Lazi%C4%87,+V.&author=Nik%C5%A1i%C4%87,+V.&author=Nedeljkovi%C4%87,+J.M.&publication_year=2025&journal=Int.+J.+Mol.+Sci.&volume=26&pages=10593&doi=10.3390/ijms262110593)**] [**CrossRef (https://doi.org/10.3390/ijms262110593)**] [**Scilit (https://www.scilit.com/publications/e0135d9751368fbc8e7a36456dc1c0b5)**]

19. Schneider, J.; Matsuoka, M.; Takeuchi, M.; Zhang, J.; Horiuchi, Y.; Anpo, M.; Bahnemann, D.W. Understanding TiO_2 photocatalysis: Mechanisms and materials. *Chem. Rev.* **2014**, *114*, 9919–9986. [**Google Scholar (https://scholar.google.com/scholar_lookup?title=Understanding+TiO2+photocatalysis:+Mechanisms+and+materials&author=Schneider,+J.&author=Matsuoka,+M.&author=Takeuchi,+M.&author=Zhang,+J.&author=Horiuchi,+Y.&author=Anpo,+M.&author=Bahnemann,+D.W.&publication_year=2014&journal=Chem.+Rev.&volume=114&pages=9919%E2%80%939986&doi=10.1021/cr5001892&pmid=25234429)**] [**CrossRef (https://doi.org/10.1021/cr5001892)**] [**Scilit (https://www.scilit.com/publications/897d5d961c255c585a052a888453d210)**] [**PubMed (https://www.ncbi.nlm.nih.gov/pubmed/25234429)**]

20. Kumar, R.; Sudhaik, A.; Raizada, P.; Hosseini-Bandegharaei, A.; Thakur, V.K.; Saini, A.; Saini, V.; Singh, P. An overview on bismuth molybdate based photocatalytic systems: Controlled morphology and enhancement strategies for photocatalytic water purification. *J. Environ. Chem. Eng.* **2020**, *8*, 104291. [**Google Scholar (https://scholar.google.com/scholar_lookup?title=An+overview+on+bismuth+molybdate+based+photocatalytic+systems:+Controlled+morphology+and+enhancement+strategies+for+photocatalytic+water+purification&author=Kumar,+R.&author=Sudhaik,+A.&author=Raizada,+P.&author=Hosseini-Bandegharaei,+A.&author=Thakur,+V.K.&author=Saini,+A.&author=Saini,+V.&author=Singh,+P.&publication_year=2020&journal=J.+Environ.+Chem.+Eng.&volume=8&pages=104291&doi=10.1016/j.jece.2020.104291)**] [**CrossRef (https://doi.org/10.1016/j.jece.2020.104291)**] [**Scilit (https://www.scilit.com/publications/4db3bdbdb120d7341cc447306ea6ab13)**]

21. Ong, W.-J.; Tan, L.-L.; Ng, Y.H.; Yong, S.-T.; Chai, S.-P. Graphitic carbon nitride ($g-C_3N_4$)-based photocatalysts for artificial photosynthesis and environmental remediation: Are we a step closer to achieving sustainability? *Chem. Rev.* **2016**, *116*, 7159–7329. [**Google Scholar (https://scholar.google.com/scholar_lookup?title=Graphitic+carbon+nitride+(g-C3N4)-based+photocatalysts+for+artificial+photosynthesis+and+environmental+remediation:+Are+we+a+step+closer+to+achieving+sustainability?&author=Ong,+W.-J.&author=Tan,+L.-L.&author=Ng,+Y.H.&author=Yong,+S.-T.&author=Chai,+S.-P.&publication_year=2016&journal=Chem.+Rev.&volume=116&pages=7159%E2%80%937329&doi=10.1021/acs.chemrev.6b00075&pmid=27199146)**] [**CrossRef (https://doi.org/10.1021/acs.chemrev.6b00075)**] [**Scilit (https://www.scilit.com/publications/7f4da2486bea1223af58fa5d9dd4fb7d)**] [**PubMed (https://www.ncbi.nlm.nih.gov/pubmed/27199146)**]

22. Cui, Z.; Wu, H.; Bai, K.; Chen, X.; Li, E.; Shen, Y.; Wang, M. Fabrication of a $g-C_3N_4/MoS_2$ photocatalyst for enhanced RhB degradation. *Phys. E Low-Dimens. Syst. Nanostructures* **2022**, *144*, 115361. [**Google Scholar (https://scholar.google.com/scholar_lookup?title=Fabrication+of+a+g-C3N4/MoS2+photocatalyst+for+enhanced+RhB+degradation&author=Cui,+Z.&author=Wu,+H.&author=Bai,+K.&author=Chen,+X.&author=Li,+E.&author=Shen,+Y.&author=Wang,+M.&publication_year=2022&journal=Phys.+E+Low-Dimens.+Syst.+Nanostructures&volume=144&pages=115361&doi=10.1016/j.physe.2022.115361)**] [**CrossRef (https://doi.org/10.1016/j.physe.2022.115361)**] [**Scilit (https://www.scilit.com/publications/046bc43f9ffd696df287be4b97fe5dbb)**]

23. Merdoud, R.; Aoudjit, F.; Mouni, L.; Honavar, V.; Moghadam, R.P.; Palabathuni, M.; Ranade, V.V. Methyl orange degradation using Ag-doped TiO_2, H_2O_2, and Hydrodynamic Cavitation. *ACS Omega* **2025**, *10*, 21377–21390. [**Google Scholar (https://scholar.google.com/scholar_lookup?title=Methyl+orange+degradation+using+Ag-doped+TiO2,+H2O2,+and+Hydrodynamic+Cavitation&author=Merdoud,+R.&author=Aoudjit,+F.&author=Mouni,+L.&author=Honavar,+V.&author=Moghadam,+R.P.&author=Palabathuni,+M.&author=Ranade,+V.V.&publication_year=2025&journal=ACS+Omega&volume=10&pages=21377%E2%80%9321390&doi=10.1021/acsomega.5c00034&pmid=40488051)**] [**CrossRef (https://doi.org/10.1021/acsomega.5c00034)**] [**Scilit (https://www.scilit.com/publications/ab541b2d2a10a2f8de17c8d97cc62be4)**] [**PubMed (https://www.ncbi.nlm.nih.gov/pubmed/40488051)**]

24. Tebbi, S.O.; Amrane, A.; Boudraa, R.; Bollinger, J.-C.; Salvestrini, S.; Kanjal, M.I.; Tiri, A.; Belkhiri, L.; Alharthi, M.N.; Mouni, L. Green synthesis of sustainable and cost-effective TiO_2-SiO_2-Fe_2O_3 heterojunction nanocomposites for rhodamine B dye degradation under sunlight. *Water* **2025**, *17*, 168. [**Google Scholar (https://scholar.google.com/scholar_lookup?title=Green+synthesis+of+sustainable+and+cost-effective+TiO2-SiO2-Fe2O3+heterojunction+nanocomposites+for+rhodamine+B+dye+degradation+under+sunlight&author=Tebbi,+S.O.&author=Amrane,+A.&author=Boudraa,+R.&author=Bollinger,+J.-C.&author=Salvestrini,+S.&author=Kanjal,+M.I.&author=Tiri,+A.&author=Belkhiri,+L.&author=Alharthi,+M.N.&author=Mouni,+L.&publication_year=2025&journal=Water&volume=17&pages=168&doi=10.3390/w17020168)**] [**CrossRef (https://doi.org/10.3390/w17020168)**] [**Scilit (https://www.scilit.com/publications/9a7e7ec0d79fc77cfde7378874813b59)**]

25. Boudraa, R.; Talantikite-Touati, D.; Souici, A.; Djermoune, A.; Saidani, A.; Fendi, K.; Amrane, A.; Bollinger, J.-C.; Tran, H.N.; Mouni, L. Breaking new grounds: Solid-state synthesis of TiO_2–La_2O_3–CuO nanocomposites for degrading brilliant green dye under visible light. *J. Clean. Prod.* **2024**, *481*, 144126. [**Google Scholar (https://scholar.google.com/scholar_lookup?title=Breaking+new+grounds:+Solid-state+synthesis+of+TiO2%E2%80%93La2O3%E2%80%93CuO+nanocomposites+for+degrading+brilliant+green+dye+under+visible+light&author=Boudraa,+R.&author=Talantikite-Touati,+D.&author=Souici,+A.&author=Djermoune,+A.&author=Saidani,+A.&author=Fendi,+K.&author=Amrane,+A.&author=Bollinger,+J.-C.&author=Tran,+H.N.&author=Mouni,+L.&publication_year=2024&journal=J.+Clean.+Prod.&volume=481&pages=144126&doi=10.1016/j.jclepro.2024.144126)**] [**CrossRef (https://doi.org/10.1016/j.jclepro.2024.144126)**] [**Scilit (https://www.scilit.com/publications/136fd96eb975d71cec9796ab8ed178a4)**]

26. You, Z.; Lu, D.; Kondamareddy, K.K.; Gu, W.; Su, Y.; Pan, J.; Yang, J.; Cheng, P.; Ho, W. Organic-inorganic PVDF/$Zn_{0.5}Cd_{0.5}S$/Ti-NT photocatalytic membrane with synergistic effect of heterojunction and its derived multi-element excitation NO purification. *Sep. Purif. Technol.* **2025**, *361*, 131293. [**Google Scholar (https://scholar.google.com/scholar_lookup?title=Organic-inorganic+PVDF/Zn0.5Cd0.5S/Ti-NT+photocatalytic+membrane+with+synergistic+effect+of+heterojunction+and+its+derived+multi-element+excitation+NO+purification&author=You,+Z.&author=Lu,+D.&author=Kondamareddy,+K.K.&author=Gu,+W.&author=Su,+Y.&author=Pan,+J.&author=Yang,+J.&author=Cheng,+P.&author=Ho,+W.&publication_year=2025&journal=Sep.+Purif.+Technol.&volume=361&pages=131293&doi=10.1016/j.seppur.2024.131293)**] [**CrossRef (https://doi.org/10.1016/j.seppur.2024.131293)**] [**Scilit (https://www.scilit.com/publications/8259f5541077432a24e2337a600d97dc)**]

27. Wen, X.; Liao, L.; He, Y.; Jin, Y.; Ren, P.; He, L.; Jiang, C.; Yuan, W. Construction and performance regulation of TiO_2/Bi_2O_3 photocatalyst with Z-scheme heterojunction. *J. Photochem. Photobiol. A Chem.* **2026**, *476*, 117074. [**Google Scholar (https://scholar.google.com/scholar_lookup?title=Construction+and+performance+regulation+of+TiO2/Bi2O3+photocatalyst+with+Z-scheme+heterojunction&author=Wen,+X.&author=Liao,+L.&author=He,+Y.&author=Jin,+Y.&author=Ren,+P.&author=He,+L.&author=Jiang,+C.&author=Yuan,+W.&publication_year=2026&journal=J.+Photochem.+Photobiol.+A+Chem.&volume=476&pages=117074&doi=10.1016/j.jphotochem.2026.117074)**] [**CrossRef (https://doi.org/10.1016/j.jphotochem.2026.117074)**] [**Scilit (https://www.scilit.com/publications/47cffc31d23d4b4e39b55699dc41b218)**]

28. Tabari, F.H.; Hamidinezhad, H. Effective photodegradation of organic pollutants and antibacterial activity by TiO_2/ZnO composite nanofibers as a direct Z-scheme heterojunction photocatalyst. *J. Water Process Eng.* **2025**, *77*, 108562. [**Google Scholar (https://scholar.google.com/scholar_lookup?title=Effective+photodegradation+of+organic+pollutants+and+antibacterial+activity+by+TiO2/ZnO+composite+nanofibers+as+a+direct+Z-scheme+heterojunction+photocatalyst&author=Tabari,+F.H.&author=Hamidinezhad,+H.&publication_year=2025&journal=J.+Water+Process+Eng.&volume=77&pages=108562&doi=10.1016/j.jwpe.2025.108562)**] [**CrossRef (https://doi.org/10.1016/j.jwpe.2025.108562)**] [**Scilit (https://www.scilit.com/publications/9b06038aa20765003b3fa66fa0174896)**]

29. Atambo, M.O.; Varsano, D.; Ferretti, A.; Ataei, S.S.; Caldas, M.J.; Molinari, E.; Selloni, A. Electronic and optical properties of doped TiO_2 by many-body perturbation theory. *Phys. Rev. Mater.* **2019**, *3*, 045401. [**Google Scholar (https://scholar.google.com/scholar_lookup?title=Electronic+and+optical+properties+of+doped+TiO2+by+many-body+perturbation+theory&author=Atambo,+M.O.&author=Varsano,+D.&author=Ferretti,+A.&author=Ataei,+S.S.&author=Caldas,+M.J.&author=Molinari,+E.&author=Selloni,+A.&publication_year=2019&journal=Phys.+Rev.+Mater.&volume=3&pages=045401&doi=10.1103/PhysRevMaterials.3.045401)**] [**CrossRef (https://doi.org/10.1103/PhysRevMaterials.3.045401)**] [**Scilit (https://www.scilit.com/publications/052ebc39cab29c09bedfd4bffd84da1d)**]

30. Kubiak, A.; Kubacka, M.; Gabała, E.; Dobrowolska, A.; Synoradzki, K.; Siwińska-Ciesielczyk, K.; Czaczyk, K.; Jesionowski, T. Hydrothermally assisted fabrication of TiO_2-Fe_3O_4 composite materials and their antibacterial activity. *Materials* **2020**, *13*, 4715. [**Google Scholar (https://scholar.google.com/scholar_lookup?title=Hydrothermally+assisted+fabrication+of+TiO2-Fe3O4+composite+materials+and+their+antibacterial+activity&author=Kubiak,+A.&author=Kubacka,+M.&author=Gaba%C5%82a,+E.&author=Dobrowolska,+A.&author=Synoradzki,+K.&author=Siwi%C5%84ska-Ciesielczyk,+K.&author=Czaczyk,+K.&author=Jesionowski,+T.&publication_year=2020&journal=Materials&volume=13&pages=4715&doi=10.3390/ma13214715)**] [**CrossRef (https://doi.org/10.3390/ma13214715)**] [**Scilit (https://www.scilit.com/publications/bae0cd3e5a6a86ab466236160128ecbb)**]

31. Low, J.; Yu, J.; Jaroniec, M.; Wageh, S.; Al-Ghamdi, A.A. Heterojunction photocatalysts. *Adv. Mater.* **2017**, *29*, 1601694. [**Google Scholar (https://scholar.google.com/scholar_lookup?title=Heterojunction+photocatalysts&author=Low,+J.&author=Yu,+J.&author=Jaroniec,+M.&author=Wageh,+S.&author=Al-Ghamdi,+A.A.&publication_year=2017&journal=Adv.+Mater.&volume=29&pages=1601694&doi=10.1002/adma.201601694)**] [**CrossRef (https://doi.org/10.1002/adma.201601694)**] [**Scilit (https://www.scilit.com/publications/93c63cfb024e5c64fc7e2b38d7ed6949)**]

32. Samarasinghe, L.V.; Muthukumaran, S.; Baskaran, K. Heterojunction photocatalysts for solar-driven wastewater treatment: Interfacial design, charge carrier dynamics, and advanced characterization techniques. *J. Water Process Eng.* **2025**, *79*, 108960. [**Google Scholar (https://scholar.google.com/scholar_lookup?title=Heterojunction+photocatalysts+for+solar-driven+wastewater+treatment:+Interfacial+design,+charge+carrier+dynamics,+and+advanced+characterization+techniques&author=Samarasinghe,+L.V.&author=Muthukumaran,+S.&author=Baskaran,+K.&publication_year=2025&journal=J.+Water+Process+Eng.&volume=79&pages=108960&doi=10.1016/j.jwpe.2025.108960)**] [**CrossRef (https://doi.org/10.1016/j.jwpe.2025.108960)**] [**Scilit (https://www.scilit.com/publications/489f269aeb115b18939d2ed11439ae59)**]

33. Mamba, G.; Mishra, A. Graphitic carbon nitride (g-C_3N_4) nanocomposites: A new and exciting generation of visible light driven photocatalysts for environmental pollution remediation. *Appl. Catal. B Environ.* **2016**, *198*, 347–377. [**Google Scholar (https://scholar.google.com/scholar_lookup?title=Graphitic+carbon+nitride+(g-C3N4)+nanocomposites:+A+new+and+exciting+generation+of+visible+light+driven+photocatalysts+for+environmental+pollution+remediation&author=Mamba,+G.&author=Mishra,+A.&publication_year=2016&journal=Appl.+Catal.+B+Environ.&volume=198&pages=347%E2%80%93377&doi=10.1016/j.apcatb.2016.05.052)**] [**CrossRef (https://doi.org/10.1016/j.apcatb.2016.05.052)**] [**Scilit (https://www.scilit.com/publications/1f69379d03bccdb5983f36e29b1c2134)**]

34. Chen, F.; Yang, Q.; Wang, Y.; Zhao, J.; Wang, D.; Li, X.; Guo, Z.; Wang, H.; Deng, Y.; Niu, C. Novel ternary heterojunction photcocatalyst of Ag nanoparticles and g-C_3N_4 nanosheets co-modified $BiVO_4$ for wider spectrum visible-light photocatalytic degradation of refractory pollutant. *Appl. Catal. B Environ.* **2017**, *205*, 133–147. [**Google Scholar (https://scholar.google.com/scholar_lookup?title=Novel+ternary+heterojunction+photcocatalyst+of+Ag+nanoparticles+and+g-C3N4+nanosheets+co-modified+BiVO4+for+wider+spectrum+visible-light+photocatalytic+degradation+of+refractory+pollutant&author=Chen,+F.&author=Yang,+Q.&author=Wang,+Y.&author=Zhao,+J.&author=Wang,+D.&author=Li,+X.&author=Guo,+Z.&author=Wang,+H.&author=Deng,+Y.&author=Niu,+C.&publication_year=2017&journal=Appl.+Catal.+B+Environ.&volume=205&pages=133%E2%80%93147&doi=10.1016/j.apcatb.2016.12.017)**] [**CrossRef (https://doi.org/10.1016/j.apcatb.2016.12.017)**] [**Scilit (https://www.scilit.com/publications/4e58638f9a213669f7ff5786f723e981)**]

35. Wang, H.; Zhang, L.; Chen, Z.; Hu, J.; Li, S.; Wang, Z.; Liu, J.; Wang, X. Semiconductor heterojunction photocatalysts: Design, construction, and photocatalytic performances. *Chem. Soc. Rev.* **2014**, *43*, 5234–5244. [**Google Scholar (https://scholar.google.com/scholar_lookup?title=Semiconductor+heterojunction+photocatalysts:+Design,+construction,+and+photocatalytic+performances&author=Wang,+H.&author=Zhang,+L.&author=Chen,+Z.&author=Hu,+J.&author=Li,+S.&author=Wang,+Z.&author=Liu,+J.&author=Wang,+X.&publication_year=2014&journal=Chem.+Soc.+Rev.&volume=43&pages=5234%E2%80%935244&doi=10.1039/C4CS00126E)**] [**CrossRef (https://doi.org/10.1039/C4CS00126E)**] [**Scilit (https://www.scilit.com/publications/2ee9e51fb13e01412b9fbf9f1f41bede)**]

36. Chowdhury, A.P.; Anantharaju, K.S.; Keshavamurthy, K.; Swain, S.; Uma, B. A mini-review on Z and S scheme heterojunction bismuth based photocatalysts towards H_2 production, CO_2 reduction, and pollutant degradation. *Next Mater.* **2025**, *8*, 100918. [**Google Scholar (https://scholar.google.com/scholar_lookup?title=A+mini-review+on+Z+and+S+scheme+heterojunction+bismuth+based+photocatalysts+towards+H2+production,+CO2+reduction,+and+pollutant+degradation&author=Chowdhury,+A.P.&author=Anantharaju,+K.S.&author=Keshavamurthy,+K.&author=Swain,+S.&author=Uma,+B.&publication_year=2025&journal=Next+Mater.&volume=8&pages=100918&doi=10.1016/j.nxmate.2025.100918)**] [**CrossRef (https://doi.org/10.1016/j.nxmate.2025.100918)**] [**Scilit (https://www.scilit.com/publications/a9054532c65bea61e4061d4fd395a2f2)**]

37. Xu, Q.; Zhang, L.; Cheng, B.; Fan, J.; Yu, J. S-scheme heterojunction photocatalyst. *Chem* **2020**, *6*, 1543–1559. [**Google Scholar (https://scholar.google.com/scholar_lookup?title=S-scheme+heterojunction+photocatalyst&author=Xu,+Q.&author=Zhang,+L.&author=Cheng,+B.&author=Fan,+J.&author=Yu,+J.&publication_year=2020&journal=Chem&volume=6&pages=1543%E2%80%931559&doi=10.1016/j.chempr.2020.06.010)**] [**CrossRef (https://doi.org/10.1016/j.chempr.2020.06.010)**] [**Scilit (https://www.scilit.com/publications/42b5ad37a7891d9f7b70a4fc8131bd8b)**]

38. Li, H.; Tu, W.; Zhou, Y.; Zou, Z. Z-Scheme photocatalytic systems for promoting photocatalytic performance: Recent progress and future challenges. *Adv. Sci.* **2016**, *3*, 1500389. [**Google Scholar (https://scholar.google.com/scholar_lookup?title=Z-Scheme+photocatalytic+systems+for+promoting+photocatalytic+performance:+Recent+progress+and+future+challenges&author=Li,+H.&author=Tu,+W.&author=Zhou,+Y.&author=Zou,+Z.&publication_year=2016&journal=Adv.+Sci.&volume=3&pages=1500389&doi=10.1002/advs.201500389)**] [**CrossRef (https://doi.org/10.1002/advs.201500389)**] [**Scilit (https://www.scilit.com/publications/49ac850c3786cdea7a552143875e7931)**]

39. Jing, H.-x.; Gao, Y.-l.; Li, L.-x.; Wang, X.; Pei, W.-j.; Yang, X.-f. Synthesis of a novel double Z-scheme TiO_2/Bi_2O_3-g-C_3N_4 photocatalyst with enhanced photocatalytic performance to rhodamine B under sunlight. *J. Clust. Sci.* **2023**, *34*, 1347–1354. [**Google Scholar (https://scholar.google.com/scholar_lookup?title=Synthesis+of+a+novel+double+Z-scheme+TiO2/Bi2O3-g-C3N4+photocatalyst+with+enhanced+photocatalytic+performance+to+rhodamine+B+under+sunlight&author=Jing,+H.-x.&author=Gao,+Y.-l.&author=Li,+L.-x.&author=Wang,+X.&author=Pei,+W.-j.&author=Yang,+X.-f.&publication_year=2023&journal=J.+Clust.+Sci.&volume=34&pages=1347%E2%80%931354&doi=10.1007/s10876-022-02308-4)**] [**CrossRef (https://doi.org/10.1007/s10876-022-02308-4)**] [**Scilit (https://www.scilit.com/publications/dbeee079dd5f563c7d646e9ccb7fe690)**]

40. Zhong, C.; Wei, W.; He, H.; Huangfu, Z.; Wang, Y.; Yu, J. The photocatalytic performance of ternary g-$C_3N_4/Bi_2O_3/TiO_2$ heterojunction composite for degradation of organic pollutants under visible and ultraviolet light. *J. Mater. Sci. Mater. Electron.* **2021**, *32*, 2146–2157. [**Google Scholar (https://scholar.google.com/scholar_lookup?title=The+photocatalytic+performance+of+ternary+g-C3N4/Bi2O3/TiO2+heterojunction+composite+for+degradation+of+organic+pollutants+under+visible+and+ultraviolet+light&author=Zhong,+C.&author=Wei,+W.&author=He,+H.&author=Huangfu,+Z.&author=Wang,+Y.&author=Yu,+J.&publication_year=2021&journal=J.+Mater.+Sci.+Mater.+Electron.&volume=32&pages=2146%E2%80%932157&doi=10.1007/s10854-020-04980-6)**] [**CrossRef (https://doi.org/10.1007/s10854-020-04980-6)**] [**Scilit (https://www.scilit.com/publications/ee57d42e8f167aa1c71f4b6fad8761f9)**]

41. Rohilla, P.; Pal, B.; Das, R.K. Improved photocatalytic degradation of rhodamine B by g-C_3N_4 loaded $BiVO_4$ nanocomposites. *Heliyon* **2023**, *9*, e21900. [**Google Scholar (https://scholar.google.com/scholar_lookup?title=Improved+photocatalytic+degradation+of+rhodamine+B+by+g-C3N4+loaded+BiVO4+nanocomposites&author=Rohilla,+P.&author=Pal,+B.&author=Das,+R.K.&publication_year=2023&journal=Heliyon&volume=9&pages=e21900&doi=10.1016/j.heliyon.2023.e21900)**] [**CrossRef (https://doi.org/10.1016/j.heliyon.2023.e21900)**] [**Scilit (https://www.scilit.com/publications/2524d46b19a35e7f24f80817fc50821f)**]

42. Peng, W.; Yang, C.; Yu, J. Bi_2O_3 and g-C_3N_4 quantum dot modified anatase TiO_2 heterojunction system for degradation of dyes under sunlight irradiation. *RSC Adv.* **2020**, *10*, 1181–1190. [**Google Scholar (https://scholar.google.com/scholar_lookup?title=Bi2O3+and+g-C3N4+quantum+dot+modified+anatase+TiO2+heterojunction+system+for+degradation+of+dyes+under+sunlight+irradiation&author=Peng,+W.&author=Yang,+C.&author=Yu,+J.&publication_year=2020&journal=RSC+Adv.&volume=10&pages=1181%E2%80%931190&doi=10.1039/C9RA07424D)**] [**CrossRef (https://doi.org/10.1039/C9RA07424D)**] [**Scilit (https://www.scilit.com/publications/048163a1b937f925249efb6110004767)**]

43. Jabbar, Z.H.; Graimed, B.H. Recent developments in industrial organic degradation via semiconductor heterojunctions and the parameters affecting the photocatalytic process: A review study. *J. Water Process Eng.* **2022**, *47*, 102671. [**Google Scholar (https://scholar.google.com/scholar_lookup?title=Recent+developments+in+industrial+organic+degradation+via+semiconductor+heterojunctions+and+the+parameters+affecting+the+photocatalytic+process:+A+review+study&author=Jabbar,+Z.H.&author=Graimed,+B.H.&publication_year=2022&journal=J.+Water+Process+Eng.&volume=47&pages=102671&doi=10.1016/j.jwpe.2022.102671)**] [**CrossRef (https://doi.org/10.1016/j.jwpe.2022.102671)**] [**Scilit (https://www.scilit.com/publications/ba1eaa171c0130c6fc486530cdd0fae5)**]

44. Bendjama, M.; Hamdaoui, O. Photocatalytic Degradation of Safranin O: Unraveling the Roles of Dissolved Gases, Environmental Matrices, and Reactive Species. *Catalysts* **2025**, *15*, 914. [**Google Scholar (https://scholar.google.com/scholar_lookup?title=Photocatalytic+Degradation+of+Safranin+O:+Unraveling+the+Roles+of+Dissolved+Gases,+Environmental+Matrices,+and+Reactive+Species&author=Bendjama,+M.&author=Hamdaoui,+O.&publication_year=2025&journal=Catalysts&volume=15&pages=914&doi=10.3390/catal15090914)**] [**CrossRef (https://doi.org/10.3390/catal15090914)**] [**Scilit (https://www.scilit.com/publications/eb29f5341ab97ab9f6a2066d3e818468)**]

45. Al Miad, A.; Saikat, S.P.; Alam, M.K.; Hossain, M.S.; Bahadur, N.M.; Ahmed, S. Metal oxide-based photocatalysts for the efficient degradation of organic pollutants for a sustainable environment: A review. *Nanoscale Adv.* **2024**, *6*, 4781–4803. [**Google Scholar (https://scholar.google.com/scholar_lookup?title=Metal+oxide-based+photocatalysts+for+the+efficient+degradation+of+organic+pollutants+for+a+sustainable+environment:+A+review&author=Al+Miad,+A.&author=Saikat,+S.P.&author=Alam,+M.K.&author=Hossain,+M.S.&author=Bahadur,+N.M.&author=Ahmed,+S.&publication_year=2024&journal=Nanoscale+Adv.&volume=6&pages=4781%E2%80%934803&doi=10.1039/D4NA00517A&pmid=39258117)**] [**CrossRef (https://doi.org/10.1039/D4NA00517A)**] [**Scilit (https://www.scilit.com/publications/a23963bc8b54839bc358472e856127d6)**] [**PubMed (https://www.ncbi.nlm.nih.gov/pubmed/39258117)**]

46. Wang, Q.; Li, Y.; Huang, F.; Song, S.; Ai, G.; Xin, X.; Zhao, B.; Zheng, Y.; Zhang, Z. Recent advances in g-C_3N_4-based materials and their application in energy and environmental sustainability. *Molecules* **2023**, *28*, 432. [**Google Scholar (https://scholar.google.com/scholar_lookup?title=Recent+advances+in+g-C3N4-based+materials+and+their+application+in+energy+and+environmental+sustainability&author=Wang,+Q.&author=Li,+Y.&author=Huang,+F.&author=Song,+S.&author=Ai,+G.&author=Xin,+X.&author=Zhao,+B.&author=Zheng,+Y.&author=Zhang,+Z.&publication_year=2023&journal=Molecules&volume=28&pages=432&doi=10.3390/molecules28010432)**] [**CrossRef (https://doi.org/10.3390/molecules28010432)**] [**Scilit (https://www.scilit.com/publications/c08d580385a313bdf67c87a5b6fab013)**]

47. Tonetto, G.M.; Ferreira, M.L. Fenton-like Catalysts Based on Supported Cu for Dyes' and Pharmaceuticals' Removal Using Only H_2O_2 and/or O_2 as Oxidants: A Review Focused on the Last 10 years. *ACS Omega* **2026**, *11*, 3667–3689. [**Google Scholar (https://scholar.google.com/scholar_lookup?title=Fenton-like+Catalysts+Based+on+Supported+Cu+for+Dyes%E2%80%99+and+Pharmaceuticals%E2%80%99+Removal+Using+Only+H2O2+and/or+O2+as+Oxidants:+A+Review+Focused+on+the+Last+10+years&author=Tonetto,+G.M.&author=Ferreira,+M.L.&publication_year=2026&journal=ACS+Omega&volume=11&pages=3667%E2%80%933689&doi=10.1021/acsomega.5c06331)**] [**CrossRef (https://doi.org/10.1021/acsomega.5c06331)**] [**Scilit (https://www.scilit.com/publications/f43acb4975283307300c2474a807bdba)**]

48. Khan, S.; Kim, D.-S.; Ullah, M.; Sadiq, M.; Muhammad, N.; Khan, M.; Noor, A.; Qayyum, S. Photocatalytic degradation of Rhodamine B dye over Ni–Cd doped and co-doped ZnO nanoparticles. *Sci. Rep.* **2025**, *15*, 31947. [**Google Scholar (https://scholar.google.com/scholar_lookup?title=Photocatalytic+degradation+of+Rhodamine+B+dye+over+Ni%E2%80%93Cd+doped+and+co-doped+ZnO+nanoparticles&author=Khan,+S.&author=Kim,+D.-S.&author=Ullah,+M.&author=Sadiq,+M.&author=Muhammad,+N.&author=Khan,+M.&author=Noor,+A.&author=Qayyum,+S.&publication_year=2025&journal=Sci.+Rep.&volume=15&pages=31947&doi=10.1038/s41598-025-17684-w)**] [**CrossRef (https://doi.org/10.1038/s41598-025-17684-w)**] [**Scilit (https://www.scilit.com/publications/eeef83e5bed46dcd19ec3dc8fba19606)**]

49. Egan, A.J. Bacterial outer membrane constriction. *Mol. Microbiol.* **2018**, *107*, 676–687. [**Google Scholar (https://scholar.google.com/scholar_lookup?title=Bacterial+outer+membrane+constriction&author=Egan,+A.J.&publication_year=2018&journal=Mol.+Microbiol.&volume=107&pages=676%E2%80%93687&doi=10.1111/mmi.13908&pmid=29315884)**] [**CrossRef (https://doi.org/10.1111/mmi.13908)**] [**Scilit (https://www.scilit.com/publications/02d338e487dec75cbbdd5418790f44cb)**] [**PubMed (https://www.ncbi.nlm.nih.gov/pubmed/29315884)**]

50. Maher, C.; Hassan, K.A. The Gram-negative permeability barrier: Tipping the balance of the in and the out. *mBio* **2023**, *14*, e01205-23. [**Google Scholar (https://scholar.google.com/scholar_lookup?title=The+Gram-negative+permeability+barrier:+Tipping+the+balance+of+the+in+and+the+out&author=Maher,+C.&author=Hassan,+K.A.&publication_year=2023&journal=mBio&volume=14&pages=e01205-23&doi=10.1128/mbio.01205-23&pmid=37861328)**] [**CrossRef (https://doi.org/10.1128/mbio.01205-23)**] [**Scilit (https://www.scilit.com/publications/a821a35c3c73a87786a2f114b28658ce)**] [**PubMed (https://www.ncbi.nlm.nih.gov/pubmed/37861328)**]

51. Bachvarova-Nedelcheva, A.; Iordanova, R.; Stoyanova, A.; Georgieva, N.; Nemska, V.; Foteva, T. Effect of B_2O_3 on the structure, properties and antibacterial abilities of Sol-Gel-Derived $TiO_2/TeO_2/B_2O_3$ powders. *Materials* **2023**, *16*, 6400. [**Google Scholar (https://scholar.google.com/scholar_lookup?title=Effect+of+B2O3+on+the+structure,+properties+and+antibacterial+abilities+of+Sol-Gel-Derived+TiO2/TeO2/B2O3+powders&author=Bachvarova-Nedelcheva,+A.&author=Iordanova,+R.&author=Stoyanova,+A.&author=Georgieva,+N.&author=Nemska,+V.&author=Foteva,+T.&publication_year=2023&journal=Materials&volume=16&pages=6400&doi=10.3390/ma16196400)**] [**CrossRef (https://doi.org/10.3390/ma16196400)**] [**Scilit (https://www.scilit.com/publications/0bd0df9c363d2d84623dc91affb8cf52)**]

52. Gnanasekaran, L.; Pachaiappan, R.; Kumar, P.S.; Hoang, T.K.; Rajendran, S.; Durgalakshmi, D.; Soto-Moscoso, M.; Cornejo-Ponce, L.; Gracia, F. Visible light driven exotic p (CuO)-n (TiO_2) heterojunction for the photodegradation of 4-chlorophenol and antibacterial activity. *Environ. Pollut.* **2021**, *287*, 117304. [**Google Scholar (https://scholar.google.com/scholar_lookup?title=Visible+light+driven+exotic+p+(CuO)-n+(TiO2)+heterojunction+for+the+photodegradation+of+4-chlorophenol+and+antibacterial+activity&author=Gnanasekaran,+L.&author=Pachaiappan,+R.&author=Kumar,+P.S.&author=Hoang,+T.K.&author=Rajendran,+S.&author=Durgalakshmi,+D.&author=Soto-Moscoso,+M.&author=Cornejo-Ponce,+L.&author=Gracia,+F.&publication_year=2021&journal=Environ.+Pollut.&volume=287&pages=117304&doi=10.1016/j.envpol.2021.117304)**] [**CrossRef (https://doi.org/10.1016/j.envpol.2021.117304)**] [**Scilit (https://www.scilit.com/publications/26365de814ead39a1207610310529e6b)**]

53. Wu, K.; Zheng, H.; Du, L.; Guo, A.; Jiang, Y.; Liu, M.; Cai, A. Magnetic biochar anchored on g-C_3N_4 nanosheets for the inactivation of *Staphylococcus aureus* via coupled capture and visible-light photocatalysis. *J. Water Process Eng.* **2024**, *59*, 104992. [**Google Scholar (https://scholar.google.com/scholar_lookup?title=Magnetic+biochar+anchored+on+g-C3N4+nanosheets+for+the+inactivation+of+Staphylococcus+aureus+via+coupled+capture+and+visible-light+photocatalysis&author=Wu,+K.&author=Zheng,+H.&author=Du,+L.&author=Guo,+A.&author=Jiang,+Y.&author=Liu,+M.&author=Cai,+A.&publication_year=2024&journal=J.+Water+Process+Eng.&volume=59&pages=104992&doi=10.1016/j.jwpe.2024.104992)**] [**CrossRef (https://doi.org/10.1016/j.jwpe.2024.104992)**] [**Scilit (https://www.scilit.com/publications/148185169264d60d6ce26a322ee7a209)**]

54. Xue, L.; Zhang, J.; Sun, M.; Wang, D.; Zhang, H.; Zhang, R.; Duan, J.; Sand, W.; Hou, B. An environment-friendly efficient visible-light photocatalyst of P, Mo co-doped TiO_2 nanoflowers hybridized with 2D porous g-C_3N_4 nanosheets for the antibacterial application. *J. Alloys Compd.* **2025**, *1044*, 182941. [**Google Scholar (https://scholar.google.com/scholar_lookup?title=An+environment-friendly+efficient+visible-light+photocatalyst+of+P,+Mo+co-doped+TiO2+nanoflowers+hybridized+with+2D+porous+g-C3N4+nanosheets+for+the+antibacterial+application&author=Xue,+L.&author=Zhang,+J.&author=Sun,+M.&author=Wang,+D.&author=Zhang,+H.&author=Zhang,+R.&author=Duan,+J.&author=Sand,+W.&author=Hou,+B.&publication_year=2025&journal=J.+Alloys+Compd.&volume=1044&pages=182941&doi=10.1016/j.jallcom.2025.182941)**] [**CrossRef (https://doi.org/10.1016/j.jallcom.2025.182941)**] [**Scilit (https://www.scilit.com/publications/3c117145e6a0c211e962f7b41a94147a)**]

55. Cong, X.; Mazierski, P.; Miodyńska, M.; Zaleska-Medynska, A.; Horn, H.; Schwartz, T.; Gmurek, M. The role of TiO_2 and g-C_3N_4 bimetallic catalysts in boosting antibiotic resistance gene removal through photocatalyst assisted peroxone process. *Sci. Rep.* **2024**, *14*, 22897. [**Google Scholar (https://scholar.google.com/scholar_lookup?title=The+role+of+TiO2+and+g-C3N4+bimetallic+catalysts+in+boosting+antibiotic+resistance+gene+removal+through+photocatalyst+assisted+peroxone+process&author=Cong,+X.&author=Mazierski,+P.&author=Miody%C5%84ska,+M.&author=Zaleska-Medynska,+A.&author=Horn,+H.&author=Schwartz,+T.&author=Gmurek,+M.&publication_year=2024&journal=Sci.+Rep.&volume=14&pages=22897&doi=10.1038/s41598-024-74147-4)**] [**CrossRef (https://doi.org/10.1038/s41598-024-74147-4)**] [**Scilit (https://www.scilit.com/publications/659877cfb99e565c9d2da8a43ac103b7)**]

56. Kariksiz, M.; Kirkik, D. Antibacterial evaluation of antibiotic-coated titanium and stainless steel implants in orthopaedic application: A dip-coating approach. *J. Orthop. Surg. Res.* **2025**, *20*, 37. [**Google Scholar (https://scholar.google.com/scholar_lookup?title=Antibacterial+evaluation+of+antibiotic-coated+titanium+and+stainless+steel+implants+in+orthopaedic+application:+A+dip-coating+approach&author=Kariksiz,+M.&author=Kirkik,+D.&publication_year=2025&journal=J.+Orthop.+Surg.+Res.&volume=20&pages=37&doi=10.1186/s13018-025-05467-y)**] [**CrossRef (https://doi.org/10.1186/s13018-025-05467-y)**] [**Scilit (https://www.scilit.com/publications/899948b1d2980707a918fa7218282ad5)**]

57. Luthfiah, A.; Permana, M.D.; Deawati, Y.; Firdaus, M.L.; Rahayu, I.; Eddy, D.R. Photocatalysis of nanocomposite titania–natural silica as antibacterial against *Staphylococcus aureus* and *Pseudomonas aeruginosa*. *RSC Adv.* **2021**, *11*, 38528–38536. [**Google Scholar (https://scholar.google.com/scholar_lookup?title=Photocatalysis+of+nanocomposite+titania%E2%80%93natural+silica+as+antibacterial+against+Staphylococcus+aureus+and+Pseudomonas+aeruginosa&author=Luthfiah,+A.&author=Permana,+M.D.&author=Deawati,+Y.&author=Firdaus,+M.L.&author=Rahayu,+I.&author=Eddy,+D.R.&publication_year=2021&journal=RSC+Adv.&volume=11&pages=38528%E2%80%9338536&doi=10.1039/D1RA07043F)**] [**CrossRef (https://doi.org/10.1039/D1RA07043F)**] [**Scilit (https://www.scilit.com/publications/df4bdf885c4a270f581713f94603210e)**]

58. Li, Y.; Wang, Q.; Huang, L.; Xu, X.; Xie, M.; Wang, H.; Huang, S.; Zhang, F.; Zhao, Z.; Yang, J. Enhanced LED-light-driven photocatalytic antibacterial by g-C_3N_4/BiOI composites. *J. Mater. Sci. Mater. Electron.* **2019**, *30*, 2783–2794. [**Google Scholar (https://scholar.google.com/scholar_lookup?title=Enhanced+LED-light-driven+photocatalytic+antibacterial+by+g-C3N4/BiOI+composites&author=Li,+Y.&author=Wang,+Q.&author=Huang,+L.&author=Xu,+X.&author=Xie,+M.&author=Wang,+H.&author=Huang,+S.&author=Zhang,+F.&author=Zhao,+Z.&author=Yang,+J.&publication_year=2019&journal=J.+Mater.+Sci.+Mater.+Electron.&volume=30&pages=2783%E2%80%932794&doi=10.1007/s10854-018-0554-3)**] [**CrossRef (https://doi.org/10.1007/s10854-018-0554-3)**] [**Scilit (https://www.scilit.com/publications/85bb02cc0469f9f7164252d75b1f1b7a)**]

Disclaimer/Publisher's Note: The statements, opinions and data contained in all publications are solely those of the individual author(s) and contributor(s) and not of MDPI and/or the editor(s). MDPI and/or the editor(s) disclaim responsibility for any injury to people or property resulting from any ideas, methods, instructions or products referred to in the content.

© 2026 by the authors. Licensee MDPI, Basel, Switzerland. This article is an open access article distributed under the terms and conditions of the **Creative Commons Attribution (CC BY) license (https://creativecommons.org/licenses/by/4.0/)**.

Share and Cite

(mailto:?&subject=From%20MDPI%3A%20%22A%20Visible-Light-Active%20TiO2%2FBi2O3%2Fg-C3N4%20Heterojunction%3A%20Synthesis%2C%20Photocatalytic%20Degradation%20of%20Rhodamine%20B%2C%20and%20Antibacterial%20Activity"&body=https://www.mdpi.com/3890666%3A%0A%0AA%20Visible-Light-Active%20TiO2%2FBi2O3%2Fg-C3N4%20Heterojunction%3A%20Synthesis%2C%20Photocatalytic%20Degradation%20

of%20Rhodamine%20B%2C%20and%20Antibacterial%20Activity%0A%0AAbstract%3A%20Ternary%20heterojunction%20photocatalysts%20enhance%20the%20separation%20and%20transport%20of%20photogenerated%20charge%20carriers%2C%20thereby%20boosting%20their%20redox%20activity%20for%20use%20in%20environmental%20and%20sustainable%20energy%20applications.%20This%20study%20focuses%20on%20the%20synthesis%20of%20a%20TiO2%2FBi2O3%2Fg-C3N4%20heterojunction%20composite%20via%20a%20ceramic%20method%20with%20TiO2%20loadings%20of%2080%25%2C%2085%25%2C%20and%2090%25%20%28denoted%2080T-BC%2C%2085T-BC%2C%20and%2090T-BC%2C%20respectively%29%20to%20investigate%20structure%26ndash%3Bproperty%26ndash%3Bperformance%20relationships%20in%20photocatalytic%20dye%20degradation.%20The%20structural%2C%20optical%2C%20and%20morphological%20properties%20of%20the%20synthesised%20materials%20were%20characterised%20using%20X-ray%20diffraction%20%28XRD%29%2C%20scanning%20electron%20microscopy%20%28SEM%29%2C%20and%20diffuse%20reflectance%20UV%26ndash%3BVis%20spectroscopy%20%28DRS%29.%20The%20photocatalytic%20performance%20was%20evaluated%20by%20measuring%20the%20degradation%20of%20Rhodamine%20B%20under%20visible%20light%20irradiation.%20Under%20optimised%20conditions%20%28pH%206%2C%20initial%20RhB%20concentration%20of%205%20mg%2FL%2C%20and%20a%20reaction%20time%20of%20120%20min%29%2C%20a%20degradation%20rate%20of%2099%25%20was%20achieved.%20Furthermore%2C%20the%20semiconductor%20demonstrated%20significant%20antibacterial%20activity%20against%20both%20Gram-negative%20%28Pseudomonas%20aeruginosa%29%20and[...])

(https://x.com/intent/tweet?text=A+Visible-Light-Active+TiO2%2FBi2O3%2Fg-C3N4+Heterojunction%3A+Synthesis%2C+Photocatalytic+Degradation+of+Rhodamine+B%2C+and+Antibacterial+Activity&hashtags=mdpicatalysts&url=https%3A%2F%2Fwww.mdpi.com%2F3890666&via=Catalysts_MDPI)

(http://www.linkedin.com/shareArticle?mini=true&url=https%3A%2F%2Fwww.mdpi.com%2F3890666&title=A%20Visible-Light-Active%20TiO2%2FBi2O3%2Fg-C3N4%20Heterojunction%3A%20Synthesis%2C%20Photocatalytic%20Degradation%20of%20Rhodamine%20B%2C%20and%20Antibacterial%20Activity%26source%3Dhttps%3A%2F%2Fwww.mdpi.com%26summary%3DTernary%20heterojunction%20photocatalysts%20enhance%20the%20separation%20and%20transport%20of%20photogenerated%20charge%20carriers%2C%20thereby%20boosting%20their%20redox%20activity%20for%20use%20in%20environmental%20and%20sustainable%20energy%20applications.%20This%20study%20focuses%20on%20the%20synthesis%20of%20%5B...%5D)

(http://www.facebook.com/sharer.php?u=https://www.mdpi.com/3890666)

(http://www.reddit.com/submit?url=https://www.mdpi.com/3890666)
(http://www.mendeley.com/import/?url=https://www.mdpi.com/3890666)

(/toggle_desktop_layout_cookie)

MDPI and ACS Style

Mouni, L.; Kasrani, O.; Kheznadji, Z.; Bouchelkia, N.; Rai, A.; Viscusi, G.; Khachay, A.; Ait Merzeg, F.; Taha, T.H.; S. El-Sayyad, G.; et al. A Visible-Light-Active $TiO_2/Bi_2O_3/g\text{-}C_3N_4$ Heterojunction: Synthesis, Photocatalytic Degradation of Rhodamine B, and Antibacterial Activity. *Catalysts* **2026**, *16*, 468. https://doi.org/10.3390/catal16050468

AMA Style

Mouni L, Kasrani O, Kheznadji Z, Bouchelkia N, Rai A, Viscusi G, Khachay A, Ait Merzeg F, Taha TH, S. El-Sayyad G, et al. A Visible-Light-Active $TiO_2/Bi_2O_3/g\text{-}C_3N_4$ Heterojunction: Synthesis, Photocatalytic Degradation of Rhodamine B, and Antibacterial Activity. *Catalysts*. 2026; 16(5):468. https://doi.org/10.3390/catal16050468

Chicago/Turabian Style

Mouni, Lotfi, Oumnia Kasrani, Zakari Kheznadji, Nasma Bouchelkia, Abdelwahab Rai, Gianluca Viscusi, Abdelhak Khachay, Farid Ait Merzeg, Tarek H. Taha, Gharieb S. El-Sayyad, and et al. 2026. "A Visible-Light-Active $TiO_2/Bi_2O_3/g\text{-}C_3N_4$ Heterojunction: Synthesis, Photocatalytic Degradation of Rhodamine B, and Antibacterial Activity" *Catalysts* 16, no. 5: 468. https://doi.org/10.3390/catal16050468

APA Style

Mouni, L., Kasrani, O., Kheznadji, Z., Bouchelkia, N., Rai, A., Viscusi, G., Khachay, A., Ait Merzeg, F., Taha, T. H., S. El-Sayyad, G., & Bendif, H. (2026). A Visible-Light-Active $TiO_2/Bi_2O_3/g\text{-}C_3N_4$ Heterojunction: Synthesis, Photocatalytic Degradation of Rhodamine B, and Antibacterial Activity. *Catalysts*, *16*(5), 468. https://doi.org/10.3390/catal16050468

Note that from the first issue of 2016, this journal uses article numbers instead of page numbers. See further details **here (https://www.mdpi.com/about/announcements/784)**.

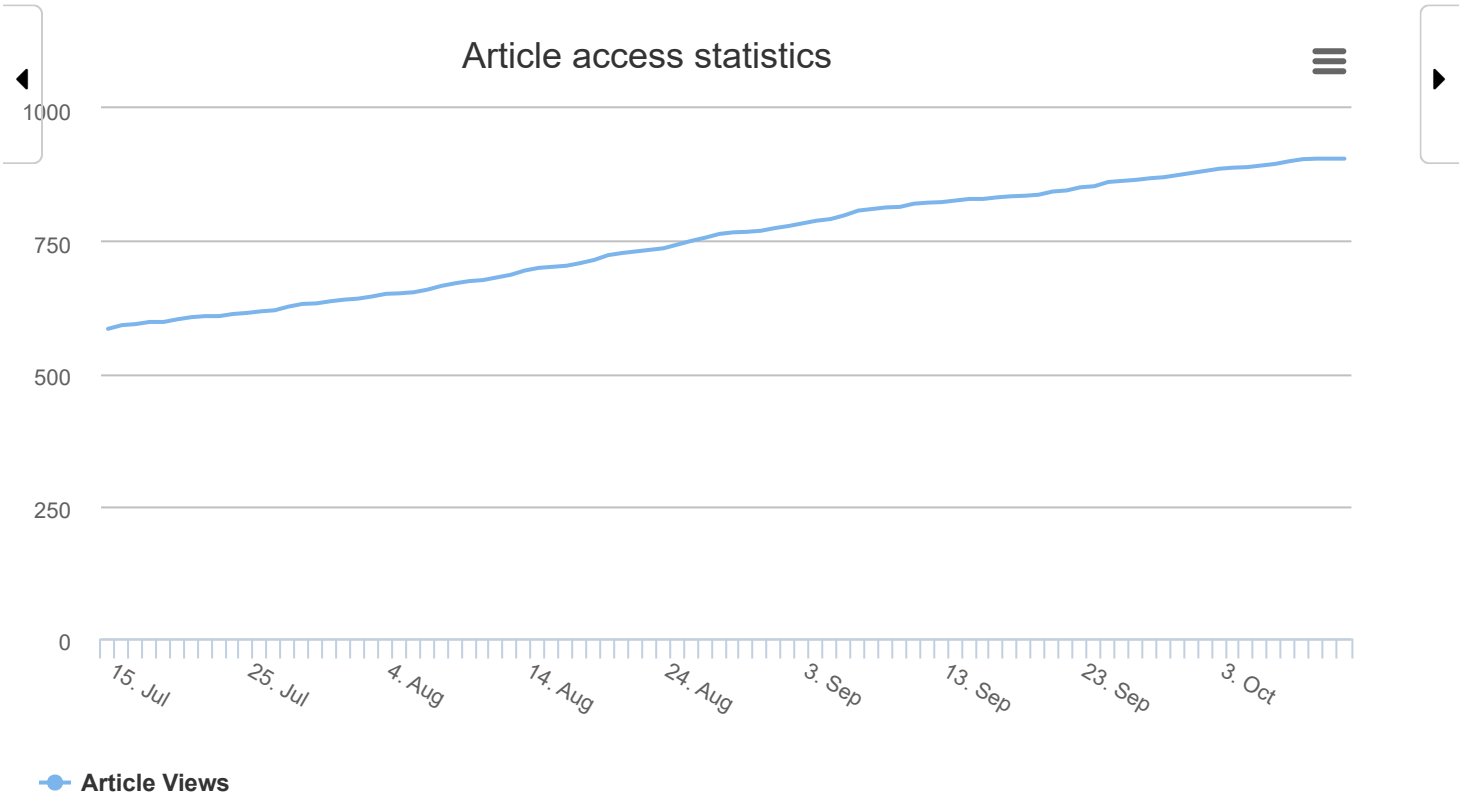
Article Metrics

Citations (/)

Crossref Scopus Web of Science Google Scholar (/toggle_desktop_layout_cookie)

7 4 (https:/
partnerID=HzO
GWVersion=2&C3N4+Heteroju

Article Access Statistics



For more information on the journal statistics, click **here (/journal/catalysts/stats)**.

Multiple requests from the same IP address are counted as one view.

***Catalysts* (/journal/catalysts)**, EISSN 2073-4344, Published by MDPI

RSS (/rss/journal/catalysts) **Content Alert (/journal/catalysts/toc-alert)**

Further Information

Article Processing Charge (/apc)

Pay an Invoice (/about/payment)

Open Access Policy (/openaccess)

Contact MDPI (/about/contact)

Jobs at MDPI (https://careers.mdpi.com)

MDPI (/)

Guidelines

For Authors (/authors)

For Reviewers (/reviewers)

For Editors (/editors)

For Librarians (/librarians)

For Publishers (/publishing_services)

For Societies (/societies)

For Conference Organizers (/conference_organizers)

(/toggle_desktop_layout_cookie)

MDPI Initiatives

Sciforum (https://sciforum.net)

MDPI Books (https://www.mdpi.com/books)

Preprints.org (https://www.preprints.org)

Scilit (https://www.scilit.com)

SciProfiles (https://sciprofiles.com?utm_source=mpdi.com&utm_medium=bottom_menu&utm_campaign=initiative)

Encyclopedia (https://encyclopedia.pub)

JAMS (https://jams.pub)

Proceedings Series (/about/proceedings)

Follow MDPI

LinkedIn (https://www.linkedin.com/company/mdpi)

Facebook (https://www.facebook.com/MDPIOpenAccessPublishing)

X (https://x.com/MDPIOpenAccess)

Subscribe to receive issue release notifications and newsletters from MDPI journals

Select options

Enter your email address...

Subscribe

© 1996-2026 MDPI (Basel, Switzerland) unless otherwise stated

MDPI (/)

Disclaimer Legal Notice (/about/legal-notice)

Terms and Conditions (/about/terms-and-conditions) Privacy Policy (/about/privacy)

Privacy Settings Accessibility (/accessibility) (/toggle_desktop_layout_cookie)